Icarus 300 (2018) 261–286

Contents lists available at ScienceDirect

Icarus

journal homepage: www.elsevier.com/locate/icarus

Late Noachian Icy Highlands climate model: Exploring the possibility of transient melting and fluvial/lacustrine activity through peak annual and seasonal temperatures

Ashley M. Palumbo[a,*], James W. Head[a], Robin D. Wordsworth[b]

[a] Department of Earth, Environmental, and Planetary Sciences, Brown University, Providence, RI 02912, USA
[b] School of Engineering and Applied Sciences, Harvard University, Cambridge, MA 02138, USA

ARTICLE INFO

Article history:
Received 20 April 2017
Revised 5 September 2017
Accepted 6 September 2017
Available online 14 September 2017

ABSTRACT

The nature of the Late Noachian climate of Mars remains one of the outstanding questions in the study of the evolution of martian geology and climate. Despite abundant evidence for flowing water (valley networks and open/closed basin lakes), climate models have had difficulties reproducing mean annual surface temperatures (MAT) > 273 K in order to generate the "warm and wet" climate conditions presumed to be necessary to explain the observed fluvial and lacustrine features. Here, we consider a "cold and icy" climate scenario, characterized by MAT ~225 K and snow and ice distributed in the southern highlands, and ask: Does the formation of the fluvial and lacustrine features require continuous "warm and wet" conditions, or could seasonal temperature variation in a "cold and icy" climate produce sufficient summertime ice melting and surface runoff to account for the observed features? To address this question, we employ the 3D Laboratoire de Météorologie Dynamique global climate model (LMD GCM) for early Mars and (1) analyze peak annual temperature (PAT) maps to determine where on Mars temperatures exceed freezing in the summer season, (2) produce temperature time series at three valley network systems and compare the duration of the time during which temperatures exceed freezing with seasonal temperature variations in the Antarctic McMurdo Dry Valleys (MDV) where similar fluvial and lacustrine features are observed, and (3) perform a positive-degree-day analysis to determine the annual volume of meltwater produced through this mechanism, estimate the necessary duration that this process must repeat to produce sufficient meltwater for valley network formation, and estimate whether runoff rates predicted by this mechanism are comparable to those required to form the observed geomorphology of the valley networks.

When considering an ambient CO_2 atmosphere, characterized by MAT ~225 K, we find that: (1) PAT can exceed the melting point of water (>273 K) in topographic lows, such as the northern lowlands and basin floors, and small regions near the equator during peak summer season conditions, despite the much lower MAT; (2) Correlation of PAT > 273 K with the predicted distribution of surface snow and ice shows that melting could occur near the edges of the ice sheet in near-equatorial regions where valley networks are abundant; (3) For the case of a circular orbit, the duration of temperatures >273 K at specific valley network locations suggests that yearly meltwater generation is insufficient to carve the observed fluvial and lacustrine features when compared with the percentage of the year required to sustain similar features in the MDV; (4) For the case of a more eccentric orbit (eccentricity of 0.17), the duration of temperatures >273 K at specific valley network locations suggests that annual meltwater generation may be capable of producing sufficient meltwater for valley network formation when repeated for many years; (5) When considering a slightly warmer climate scenario and a circular orbit, characterized by MAT ~243 K, we find that this small amount of additional greenhouse warming (~18 K MAT increase) produces time durations of temperatures >273 K that are similar to those observed in the MDV. Thus, we suggest that peak daytime and seasonal temperatures exceeding 273 K could form the valley networks and lakes with either a relatively high eccentricity condition or a small amount of additional atmospheric warming, rather than the need for a sustained MAT at or above 273 K.

* Corresponding author.
E-mail address: ashley_palumbo@brown.edu (A.M. Palumbo).

https://doi.org/10.1016/j.icarus.2017.09.007

The results from our positive-degree-day analysis suggest that: (1) For the conditions of 25° obliquity, 600 mbar atmosphere, and eccentricity of 0.17, this seasonal melting process would be required to continue for ~(33–1083) × 10^3 years to produce a sufficient volume of meltwater to form the valley networks and lakes; (2) Similarly, for the conditions of 25° obliquity, 1000 mbar atmosphere, circular orbit, and ~18 K additional greenhouse warming, the process would be required to continue for ~(21–550) × 10^3 years. Therefore, peak seasonal melting of snow and ice could induce the generation of meltwater and fluvial and lacustrine activity in a "cold and icy" Late Noachian climate in a manner similar to that observed in the MDV. A potential shortcoming of this mechanism is that independent estimates of the required runoff rates for valley network formation are much higher than those predicted by this mechanism when considering a circular orbit, even when accounting for additional atmospheric warming. However, we consider that a relatively higher eccentricity condition (0.17) may produce the necessary runoff rates: for the perihelion scenario in which perihelion occurs during southern hemispheric summer, intense melting will occur in the near-equatorial regions and in the southern hemisphere, producing runoff rates comparable to those required for valley network formation (~mm/day). In the opposite perihelion scenario, the southern hemisphere will experience very little summertime melting. Thus, this seasonal melting mechanism is a strong candidate for formation of the valley networks when considering a relatively high eccentricity (0.17) because this mechanism is capable of (1) producing meltwater in the equatorial region where valley networks are abundant, (2) continuously producing seasonal meltwater for the estimated time duration of valley network formation, (3) yielding the amount of meltwater necessary to incise the valley networks within this time period, and (4) by considering a perihelion scenario in which half of the duration of valley network formation is spent with peak summertime conditions during perihelion in each hemisphere, higher runoff rates are produced than in a circular orbit and the rates may be comparable to those required for valley network formation.

1. Introduction

Ancient fluvial features observed on the surface of Mars, including valley networks (Fassett and Head, 2008b; Hynek et al., 2010), open-basin lakes and closed-basin lakes (e.g. Fassett and Head, 2008a; Goudge et al., 2015), are indicative of the presence of significant liquid water and the occurrence of related fluvial and lacustrine processes on the surface of the southern highlands during the Late Noachian. Geologists have long argued that these features and the implied causative processes require a "warm and wet" climate, with pluvial (rainfall) activity, runoff, fluvial incision, lacustrine collection of water, and even the possible presence of oceans in the northern lowlands (e.g., Craddock and Howard, 2002; Clifford and Parker, 2001; and summary in Carr, 1999). Here we address the question: Does the Late Noachian geologic record require long-term "warm and wet" clement conditions, with temperatures consistently above the melting point of water, or can the observed fluvial/lacustrine features form through transient (seasonal) warming and melting in a "cold and icy" Late Noachian climate?

Earlier studies have explored the stability of liquid water on the surface at various times in martian history. For example, Richardson and Mischna (2005) employed the Geophysical Fluid Dynamics Laboratory (GFDL) Mars general circulation model (GCM) (Wilson and Hamilton, 1996; Wilson and Richardson, 2000; Fenton and Richardson, 2001; Richardson and Wilson, 2002; Mischna et al., 2003) to "examine scenarios corresponding to the middle and recent climate states of Mars…to find locations where conditions are acceptable for liquid water", focusing predominantly on gully formation in recent martian history. They varied the orbital parameters, forcing the pattern of solar heating (obliquity, eccentricity and argument of perihelion), and also varied the mean surface pressure in specific simulations (see their Table 1 for the parameters they used). We follow a similar approach in our analysis. In contrast to our analysis, however, Richardson and Mischna (2005) (1) did not examine the predicted water cycle because of the additional complexity and because the primary focus and conclusions of their work do not require it, (2) do not treat the radiative effects of water vapor (this is likely to become important at higher pressures and would increase greenhouse-effected surface temperatures), (3) do not account for the radiative effects of clouds, and (4) do not account for the decreased solar luminosity characteristic of the faint and young Sun, which likely would have altered their results. Their model does include an active seasonal CO_2 cycle and they treat radiative heating within the atmosphere (by dust and CO_2 gas) by using a band model approach. The CO_2 thermal infrared scheme of Hourdin (1992) is used up to 10^5 Pa in order to make a qualitative assessment of the impact of very high pressures on transient liquid water potential (TLWP); they place no quantitative emphasis on the relationship between specific mean surface pressure and resulting greenhouse warming.

Richardson and Mischna (2005) found that "liquid water is not currently stable on the surface of Mars; however, transient liquid water (ice melt) may occur if the surface temperature is between the melting and boiling points." The large diurnal range of surface temperatures means that such conditions are met on Mars with current surface pressures and obliquity, yielding the potential for transient, non-equilibrium liquid water. They then use their GCM to perform an initial exploration of the variation of this TLWP for a wide range of obliquities and increased pressures, designed to progressively explore "middle and recent climate states" of the geological history of Mars, while not attempting to recreate any particular climatological epochs. They find that at higher obliquities and slightly higher surface pressures, TLWP conditions are met over a very large fraction of Mars, but that as surface pressure is increased (> ~50–100 mbar), increased atmospheric thermal blanketing reduces the diurnal surface temperature range, eliminating the possibility of transient liquid water. On the other hand, they find that at high enough pressures (for example, 1200 mbar), the mean annual temperature is sufficiently elevated to allow stable liquid water. Thus, one of their fundamental conclusions about the "middle and recent climate states of Mars" is that "the potential for liquid water on Mars has not decreased monotonically over planetary history as the atmosphere was lost…. Instead, a distinct minimum in TLWP (the "dead zone") will have occurred during the extended period for which pressures were in the middle range between about 0.1 and 1 bar…following the earliest stages of martian evolution possibly consisting of the "warm, wet" period…". Thus, for model simulations with atmospheric pressure and spin-axis conditions comparable to conditions that may have persisted in the Noachian (1200 mbar, 25° obliquity),

Richardson and Mischna (2005) predict a "warm and wet" climate, characterized by continuous conditions suitable to the stability of liquid water on the surface.

In contrast to these findings, more recent global climate models (Forget et al., 2013; Wordsworth et al., 2013) have found that under the influence of a younger Sun, characterized by approximately 75% the current luminosity (Gough, 1981), early Mars would be characterized by an extremely cold steady-state with MAT well below the triple point of water (MAT ~225 K). In these models (described below), specific greenhouse gases and CO_2 clouds are incapable of producing the additional atmospheric and surface temperature increase necessary to cause consistent "warm and wet" conditions (MAT > 273 K), with persistent rainfall and runoff, and at the same time, remain within reasonable climate warming source and sink constraints (e.g. Forget et al., 2013; Wordsworth et al., 2013; Wordsworth et al., 2015; Kasting et al., 1992; Wolf and Toon, 2010; Halevy and Head, 2014). Although spin-axis/orbital parameter variations also differed in the past (Laskar et al., 2004), Forget et al., (2013) and Wordsworth et al., (2013) found that the range of these parameters does not induce a sufficiently large temperature increase to permit the continuous existence of stable liquid water at the surface.

Due to these difficulties in producing relatively continuous natural clement (MAT > 273 K) conditions (Forget et al., 2013; Wordsworth et al., 2013) typical of a "warm and wet" early Mars climate (e.g., Craddock and Howard, 2002), we first discuss the detailed nature of a "cold and icy" background climate, and how periods of episodic or punctuated heating might permit transitory rainfall or snowmelt, surface runoff, and fluvial/lacustrine processes. Recent GCM studies (Forget et al., 2013; Wordsworth et al., 2013) show that when atmospheric pressure exceeds tens to hundreds of millibars, an altitude-dependent temperature effect is induced and H_2O preferentially accumulates in the southern highlands, producing the conditions described by the "Late Noachian Icy Highlands" scenario (Wordsworth et al., 2013; Head and Marchant, 2014). In this context, Wordsworth et al. (2015) studied where precipitation would occur under a natural "cold and icy" scenario compared to a gray-gas/increased solar flux-forced "warm and wet" scenario; they found that snow accumulation in a "cold and icy" climate is better correlated with the known valley network distribution than pluvial (rainfall) activity in a "warm and wet" climate because the valley networks and open- and closed-basin lakes are commonly observed at distal portions of the predicted ice sheet (Head and Marchant, 2014), where melting and runoff would be expected to occur. However, surface temperatures greatly in excess of the 225 K "cold and icy" climate MAT must occur (Forget et al., 2013; Wordsworth et al., 2013) in order to induce melting of the accumulated surface snow and ice and fluvial/lacustrine activity (Head and Marchant, 2014; Fastook and Head, 2015; Rosenberg and Head, 2015).

Several candidates for transient atmospheric warming processes on a "cold and icy" early Mars (MAT ~225 K) have been proposed, including:

(1) Intense punctuated volcanism. In this scenario, periods of intense volcanism release high concentrations of sulfur dioxide into the atmosphere (Postawko and Kuhn, 1986; Mischna et al., 2013; Halevy et al., 2007; Halevy and Head, 2014). Punctuated volcanism raises temperatures enough to permit snowmelt and runoff on the surface from the increased SO_2 in the atmosphere. However, Halevy and Head (2014) point out (in agreement with Kerber et al. (2015)) that the period of warmth would be relatively short-lived, lasting decades to centuries, because the SO_2 would rapidly convert into aerosols and initiate planetary cooling.

(2) Impact crater-induced warming. Segura et al. (2002, 2008, 2012) and Toon et al. (2010) point out that impact cratering events can induce extremely high atmospheric temperatures and intense precipitation through a transient hydrologic cycle which could last hundreds of years for basin-scale impacts (Segura et al., 2002, 2008). The rainfall and runoff resulting from this mechanism are predicted to be at very high rates and globally distributed. The regionalized distribution of valley networks and their somewhat delicate dendritic nature (Hynek et al., 2010) appear to be at odds with the predicted persistent downpours and very high runoff rates (Palumbo and Head, 2017a; Wordsworth, 2016).

(3) Mean annual temperatures (MAT), peak annual temperatures (PAT) and peak daytime temperatures (PDT). In this study, we test the hypothesis that transient PDT warming in a "cold and icy" climate could cause sufficient ice melting and surface runoff to explain the observed fluvial and lacustrine features. We focus on PDT in conjunction with MAT because significant daily and seasonal variability can occur in any climate system (see Table 1 for acronym definitions). Although MAT is much less than 273 K in a "cold and icy" climate scenario, it is possible that the warmest summertime conditions may be characterized by temperatures > 273 K, permitting transient periods of ice melting and surface runoff. Thus, we explore the possibility that the ability to form fluvial and lacustrine features in a "cold and icy" climate may be defined by the duration of summertime temperatures > 273 K.

A similar approach to this was taken in a study by Richardson and Mischna (2005) in an analysis of seasonal temperature variation and the potential of seasonal ice melting and gully formation in the Amazonian. Richardson and Mischna (2005) find seasonal temperature variations to be important throughout the Amazonian, with summertime pressure and temperature conditions suitable for the presence of liquid water. They explore a range of obliquity and pressure conditions, some of which may be applicable to the Noachian, but state that they have not attempted to recreate particular climatological epochs. The Richardson and Mischna (2005) model over-predicts the greenhouse effect for pressures greater than a few hundred millibars (see their Fig. 2 caption; their GCM over-predicts temperatures by ~55 K MAT for pressure conditions ~1 bar in the 1-D Kasting Model; Kasting, 1991). This large artificial increase in MAT significantly affects the results of their higher pressure simulations. Thus, when Richardson and Mischna (2005) consider pressure and obliquity conditions representative of a Noachian climate (25° obliquity and 1200 mbar), their results are affected by the over-prediction of greenhouse warming for these high pressures. Additionally, Richardson and Mischna (2005) retain solar luminosity at the same value as today in these simulations, in contrast to predictions for solar conditions in the Noachian (Gough, 1981) (Faint Young Sun; ~75% current solar luminosity), which also forces a warmer climate.

This pioneering study has highlighted the importance of seasonal temperature variation on recent Mars (Richardson and Mischna, 2005). In our study, we utilize an updated model to extend the analysis of martian seasonal temperature variation to the Noachian, exploring a specific parameter space that is characteristic of the Noachian to effectively recreate this particular climatological epoch. We address the role of seasonal temperature variation in the Noachian and how it relates to the melting of surface snow and ice, runoff, and valley network formation.

The parameter space explored here includes variations in obliquity, pressure, and eccentricity; Richardson and Mischna (2005) also explored the influence of these parameters on the distribution of temperatures in their analysis of the recent martian

Table 1
Important abbreviations utilized in this paper. In this paper, we focus on seasonal and diurnal temperature variations, as illustrated in Fig. 1. For convenience, we will utilize multiple abbreviations in our analysis, all of which are described in the table.

Mean annual temperature (MAT)	The average temperature throughout the entire year at a specified latitude and longitude. Global MAT is the average temperature throughout the entire year for the whole globe. For example, a nominal "cold and icy" climate has global MAT of ~225 K (e.g. Wordsworth et al., 2013).
Peak annual temperature (PAT)	The warmest temperature experienced throughout the year at a specified longitude and latitude. In other words, PAT corresponds to the warmest "data point" from the GCM simulation.
Peak daytime temperature (PDT)	The warmest temperature reached within a given day at a specified latitude and longitude. We use this term when discussing diurnal temperature variation. For example, the PDT for a day in the middle of the winter will be much colder than the PDT for a day in the middle of the summer.
Mean seasonal temperature (MST)	The average temperature throughout one of the four seasons at a specified latitude and longitude. To illustrate this, consider a fictional example of a region with MAT below the melting point of water. In this case, liquid water will not be stable on the surface throughout the year. However, summertime conditions will be warmer than annual averages, and it is possible that summertime MST are above 273 K, permitting the stability of liquid water at the surface for at least half of the summer season.
Peak seasonal temperature (PST)	The maximum temperature reached throughout a specific season. We collect GCM data every six model hours, so this value represents the absolute warmest six hours of the specific season.
Positive degree day (PDD)	For the purpose of this analysis, we consider a day to be a PDD if it has at least 6 consecutive hours with an average temperature above 273 K (in other words, one data point).

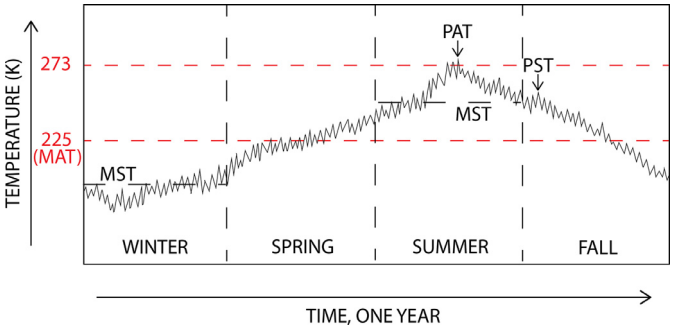

Fig. 1. A cartoon illustrating the relationship among mean annual temperatures (MAT), peak annual temperatures (PAT), mean seasonal temperatures (MST), and peak seasonal temperatures (PST). PAT can be much higher than MAT, reflecting the absolute warmest time recorded during the year. Additionally, MST can be much higher than MAT (as shown here for the summer season), or much lower (as shown here for the winter season). This example is a possible sketch for a MAT of 225 K, typical for a Late Noachian "cold and icy" climate scenario. Note that the warmest days of the summer season (PAT) experience temperatures > 273 K.

climate. Their simulation with spin-axis and pressure conditions similar to the Noachian (their simulation p128x_std: conditions of 25° obliquity and 1200 mbar CO_2 atmosphere) produces warm conditions with temperatures consistently above the melting point of water and continuous stability of liquid water at the surface. We suggest that these results are related to the nature of their model, which causes over-prediction of temperatures for the reasons outlined above (e.g. over-effective greenhouse warming, assumption of current solar luminosity, and not accounting for radiative effects of CO_2 or H_2O clouds). In this analysis, we consider the ambient "cold and icy" conditions which are predicted by our updated model, in which temperatures only exceed 273 K in the warmest hours of the summer season in a few places on the planet. The duration and distribution of these temperature conditions with respect to obliquity, pressure, and eccentricity are of critical importance to our analysis.

In order to better understand seasonal temperature variations on early Mars, we must first consider conditions on Earth. The Earth's current global MAT is ~287 K, but local MAT can reach 330 K in the hottest deserts and plummet as low as 184 K in Antarctica, at the South Pole. Thus, in addition to MAT, it is useful to explore peak temperatures, the range of temperatures, and how they vary with season (Fig. 1). In addition to MAT, we suggest that it is also important to explore peak annual temperature (PAT; the highest daily temperature reached in a year), mean seasonal temperatures (MST; for example, MAT could be well below 273 K, but MST > 273 K for the summer season), peak daily temperature (PDT; the highest temperature reached in each day), and peak seasonal temperature (PST; the highest temperature reached in each season). All abbreviations utilized in this analysis, such as those previously mentioned, are included in Table 1 with corresponding definitions.

In the Antarctic McMurdo Dry Valleys (MDV), for example, MAT (~253 K) is well below the melting point of water (273 K), yet PAT can exceed 273 K (e.g. Head and Marchant, 2014). Indeed, peak daytime temperatures (PDT) can exceed 273 K for many weeks of southern summer, top-down melting of snow and ice can occur, and resultant meltwater-related fluvial and lacustrine activity can produce observable landforms and deposits, all in the absence of pluvial activity (Marchant and Head, 2007; Head and Marchant, 2014). Over much of the MDV in southern summer, PDT can exceed 273 K, but there is commonly no surface snow and ice to melt, and the duration of the period > 273 K is insufficient for the warming thermal wave to penetrate the dry active layer and melt the ice-cemented portion of the cryosphere (Head and Marchant, 2014). Thus, formation of the fluvial and lacustrine features in the Mars-like hyperarid-hypothermal environment of the MDV requires not only PDT exceeding 273 K, but also the presence of localized surface deposits of snow and ice to melt (Head and Marchant, 2014). We use the MDV as a guideline for conditions that need to persist in a "cold and icy" early Mars climate in order for the observed martian fluvial/lacustrine features to form (Palumbo and Head, 2017b).

A factor in transient melting of the tops of cold-based glaciers in the MDV is changes in the ice albedo related to deposits on the snow and ice (Chinn, 1986; Fountain et al., 1999; Aitkins and Dickinson, 2007; Marchant and Head, 2007; Head and Marchant, 2014). The presence of rocks, dust and dirt on the ice deposit decreases the albedo of the "dirty" ice deposit, in turn increasing the amount of solar radiation absorbed by the "dirty" ice, potentially producing meltwater at surface air temperatures lower than 273 K, depending on the thickness of the deposit and other factors (Wilson and Head, 2009) which are not well constrained for the Noachian environment. The dust particles themselves will warm from solar radiation and possibly melt surrounding ice. Dust (including volcanic tephra) may have influenced ice in the Noachian (Cassanelli et al., 2015; Wilson and Head, 2009). This topic is not included in this analysis but is currently being assessed.

Additionally, Gooseff et al. (2017) have analyzed the influence of an anomalously warm year, 2002, on the physical and ecological states of the MDV. They find that the uncharacteristically warm summertime temperatures produced a significant response in the Antarctic system, with increases in lake levels and stream fluxes.

This anomalously warm year has proven to be a turning point in the MDV climate: the climate was cooling before 2002, and has been warming since 2002. While some factors in the MDV system experienced delayed responses to the 2002 austral summer, such as microbial mats and select species of Antarctic nematodes, the rivers and lakes appeared to have an immediate response, with lake levels and stream fluxes increasing immediately during the 2002 austral summer. Thus, we must also consider that anomalously warm years, such as the conditions experienced in 2002 in the MDV, may be sufficient to induce significant transient overland flow and contribute to the formation of fluvial features in a comparable Noachian climate scenario.

To address our question regarding potential seasonal melting in the "Late Noachian Icy Highlands" (LNIH) climate model, we use the 3-Dimensional Laboratoire de Météorologie Dynamique (LMD) GCM for early Mars to explore the hypothesis that peak annual, daytime or seasonal temperatures (PAT, PDT, or PST) in a "cold and icy" Late Noachian climate (Forget et al., 2013; Wordsworth et al., 2013) with MAT ~225 K could produce transient snowmelt and subsequent runoff in sufficient quantities and at the appropriate locations to explain the nature and distribution of valley networks and related lacustrine features. We focus on several specific questions: (1) In past Mars climate history when the MAT is predicted to be <<273 K, do temperatures ever exceed 273 K, for example, in the summer season? (2) If seasonal temperatures exceed 273 K in the MAT ~225 K scenario, but are insufficient to induce prolonged pluvial (rainfall) activity, are peak annual and peak seasonal temperatures (PAT/PST) sufficiently high and of a sufficient duration to cause melting of surface snow and ice? (3) How much meltwater is produced through this mechanism annually and how does this compare to the volume of water and runoff rates required to form the valley networks?

2. Methods and approaches

2.1. General model features

To complete our study, we used the 3D LMD GCM for early Mars (e.g. Wordsworth et al., 2013; Forget et al., 2013). This finite-difference model uses atmospheric radiative transfer, meteorological equations, and physical parameterizations in conjunction with one another. The model incorporates cloud microphysics with a fixed cloud condensation nuclei number density scheme for H_2O and CO_2 cloud particles (Wordsworth et al., 2013; Forget et al., 2013), convective processes (Wordsworth et al., 2013; Forget et al., 2013), and precipitation (Wordsworth et al., 2015; following Boucher et al., 1995).

Because of the uncertainties in the nature and distribution of Noachian dust, we do not include the effects of a dusty snow and ice layer here, although we recognize that the addition of dust in our simulations may aid in seasonal melting in a "cold and icy" climate (Clow, 1987; Cassanelli et al., 2015). Additionally, Kreslavsky and Head (2000, 2003, 2006) have highlighted the importance of surface slopes in seasonal melting. We acknowledge that the difference of incident solar radiation between equator-facing and pole-facing slopes may be substantial. The GCM uses MOLA topography data to account for regional slope variation, however, the resolution of the model utilized here precludes us from exploring the influence of this in more detail, and is a topic of future work.

For the purpose of this study, we track surface temperature and H_2O ice with a spatial resolution of $64 \times 48 \times 18$ (longitude $\times$ latitude $\times$ altitude), which is a sufficient spatial resolution to capture the necessary regional temperature variations, and collect hourly data, which is a sufficient temporal resolution to capture diurnal and seasonal temperature variation.

2.2. Approaches and specific applications

We employ the LMD GCM to test for transient melting under the conditions of PAT. In this analysis, we focus on a range of pressures (600–1000 mbar) for a pure CO_2 atmosphere (e.g. Forget et al., 2013), and we explore the effects of a range of spin-axis obliquities (25°–55°; $\pm 1\sigma$ of the mean obliquity over the past 5 billion years as estimated through a statistical analysis by Laskar et al., 2004) and eccentricities (0–0.17; lower and upper limit represent statistically probable values for the past 5 billion years with eccentricity 0.17 having ~20% probability; Laskar et al., 2004), assuming a solar luminosity 75% of the current value (Gough, 1981; Sagan and Mullen, 1972). It is important to note that Laskar et al. (2004) considered a statistical model, estimating probable mean values and ranges (one standard deviation) for spin-axis/orbital parameters. However, it is probable that these parameters, such as obliquity and eccentricity, varied to values outside the statistically probable range. We recognize that there was likely to be more variation than that suggested by the statistical analysis performed by Laskar et al. (2004), but for the purpose of this study we focus on the range estimated by Laskar et al. (2004), as described above.

We specifically analyze 600 mbar, 800 mbar, and 1000 mbar atmospheres, each at obliquities of 25°, 35°, 45°, and 55° and eccentricities of 0 (circular) and 0.17. In exploring this parameter space, we utilize surface temperature variation as a proxy to assess whether transient melting of snow and ice could be responsible for valley network formation in areas where Late Noachian snow accumulation is well correlated with the valley network distribution (Wordsworth et al., 2015). We also consider the addition of a small amount of greenhouse gas surrogate in the atmosphere, an addition that serves to strengthen the annual warming effect, to assess how much annual warming above 273 K could occur under conditions where MAT is greater than 225 K but still below 273 K. In this part of our analysis, our goal is to assess a climate scenario that is warmer than the baseline "cold and icy" climate (~225 K MAT), but still not continuously "warm and wet" (MAT > 273 K); this climate scenario is still broadly characterized by ice and snow distributed in the highlands and MAT far below the melting point of water. Because of uncertainty in sources and sinks for specific greenhouse gases, we account for additional greenhouse warming by adding gray gas, which absorbs evenly across the spectrum at a defined absorption coefficient. We choose a small absorption coefficient to raise MAT by only a few degrees, maintaining an overall "cold and icy" climate scenario. Lastly, we also explore additional scenarios for completeness and to consider extreme conditions, including a low obliquity (15°) simulation and a high eccentricity simulation (0.2; estimated maximum value reached in the past 5 billion years based on the statistical analysis of Laskar et al., 2004).

Seasonal temperature variation has been proven to be important in the recent Mars climate scenario (Richardson and Mischna, 2005). In our analysis we are using a more advanced model, including a water cycle, radiative effects of CO_2 and H_2O clouds, and decreased solar luminosity, to adequately test whether this importance extends throughout martian history and back to the Noachian. These results also lay the basis for determining whether repetitive yearly peak temperature melting events, in similar locations over long periods of time, could be responsible for more significant fluvial/lacustrine activity if yearly amounts of melting are insufficient to explain the entire valley network landscape, a situation that is observed in the MDV (Head and Marchant, 2014).

In this analysis, we first search for regions with substantial snow accumulation that also have PAT > 273 K, permitting snowmelt and runoff at these locations. By comparing regions of PAT > 273 K and the predicted LNIH ice distribution, we place further constraints on the spin-axis/orbital parameter space

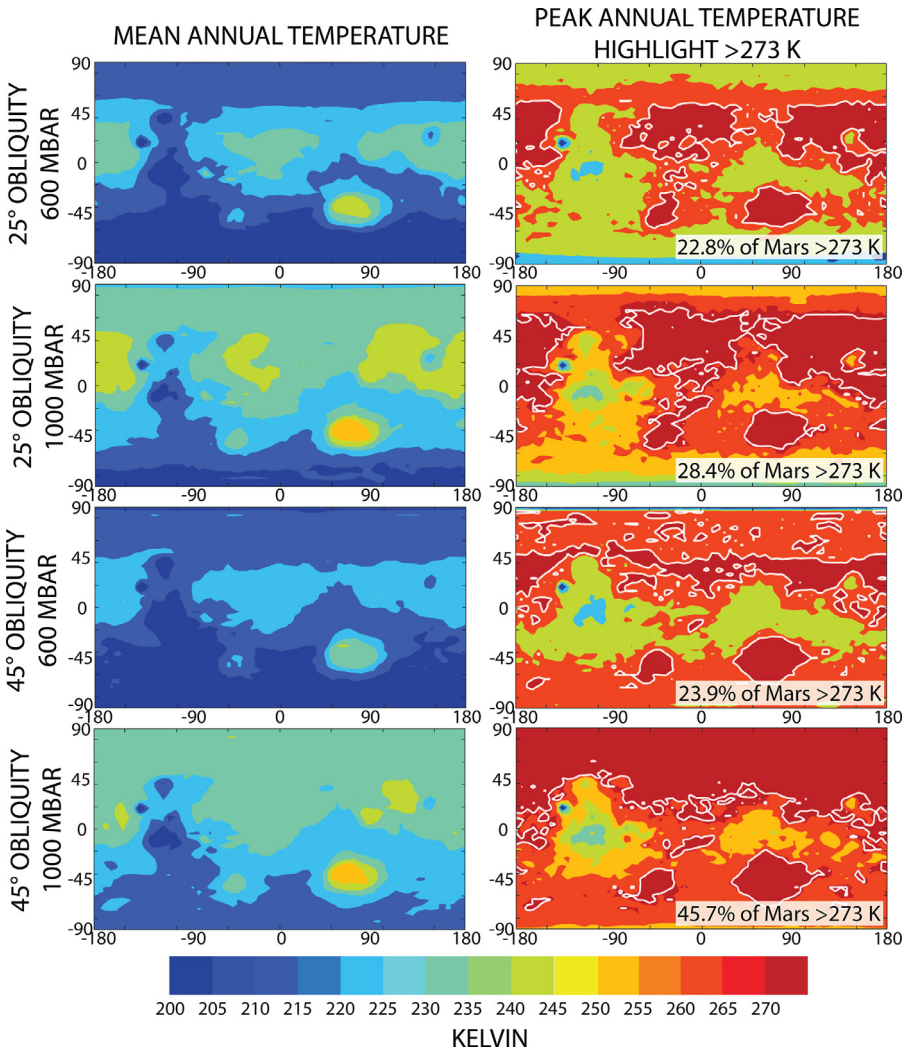

Fig. 2. Global maps of the mean (column A) and peak (maximum) (column B) annual temperature for a pure CO_2 atmosphere and a circular orbit. Shown are these mean and maximum values in conditions of different obliquity (rows 1 and 2 at 25° obliquity; rows 3 and 4 at 45° obliquity) and different atmospheric pressure (rows 1 and 3 at 600 mbar; rows 2 and 4 at 1000 mbar). Column B also shows regions with peak annual temperature > 273 K outlined in white. The purpose of this is to highlight regions with peak temperatures above the melting point of water. All data shown here are taken from model year 10. Note (1) the increase in surface area > 273 K as atmospheric pressure increases and (2) the north poleward shift of warm temperatures as obliquity increases. Column B illustrates the fact that the highest percentage of the equatorial region with PAT > 273 K occurs for low obliquity (25°) and high atmospheric pressure (1000 mbar). Although higher obliquity conditions (45°) for the same atmospheric pressure (1000 mbar) produces a higher percentage of the planet with peak annual temperatures above 273 K, we consider the lower obliquity case as optimal conditions for valley network formation because more of the equatorial region experiences peak annual temperatures > 273 K.

necessary to maximize any transient melting in the equatorial regions where valley networks are abundant. Next, we determine the annual duration of melt conditions at specific valley network systems to constrain better the applicability of this mechanism to valley network formation. The valley network systems chosen for this study are distributed near the edges of the predicted ice sheet and are locations that would require melting of ice and surface runoff to form in the "cold and icy" climate scenario. Last, we estimate the volume of meltwater produced annually through this mechanism (for optimal spin-axis/orbital and atmospheric pressure conditions). We then compare this with the total water volume believed to be required to form the valley networks and lakes to predict the total duration necessary for such a meltwater process to form these features. We also explore the magnitude of runoff rates produced by this mechanism to hypothesize whether they would be sufficient to form the valley networks and further narrow down which spin-axis/orbital and atmospheric pressure conditions are most suitable to valley network formation.

In summary, we use the 3D LMD GCM to better understand the role of seasonal temperature variations and the potential for the production of meltwater during peak summertime conditions. We explore climate variation and possible formation of fluvial and lacustrine features in a manner similar to how they form in the MDV; we do this by focusing on peak instead of mean annual temperatures and assessing whether warm summertime conditions could produce a significant quantity of meltwater. Additionally, we offer an expansion on the previously explored parameter space of early Mars climate (e.g. Richardson and Mischna, 2005; Forget et al., 2013; Wordsworth et al., 2013; Wordsworth et al., 2015) by studying the implications for both variations in eccentricity and moderate greenhouse warming in a "cold and icy" climate.

3. Analysis

We now explore the parameter space for specific spin-axis/orbital conditions, namely both 25° and 45° obliquities, each with 600 and 1000 mbar CO_2 atmospheres, at eccentricities 0 and

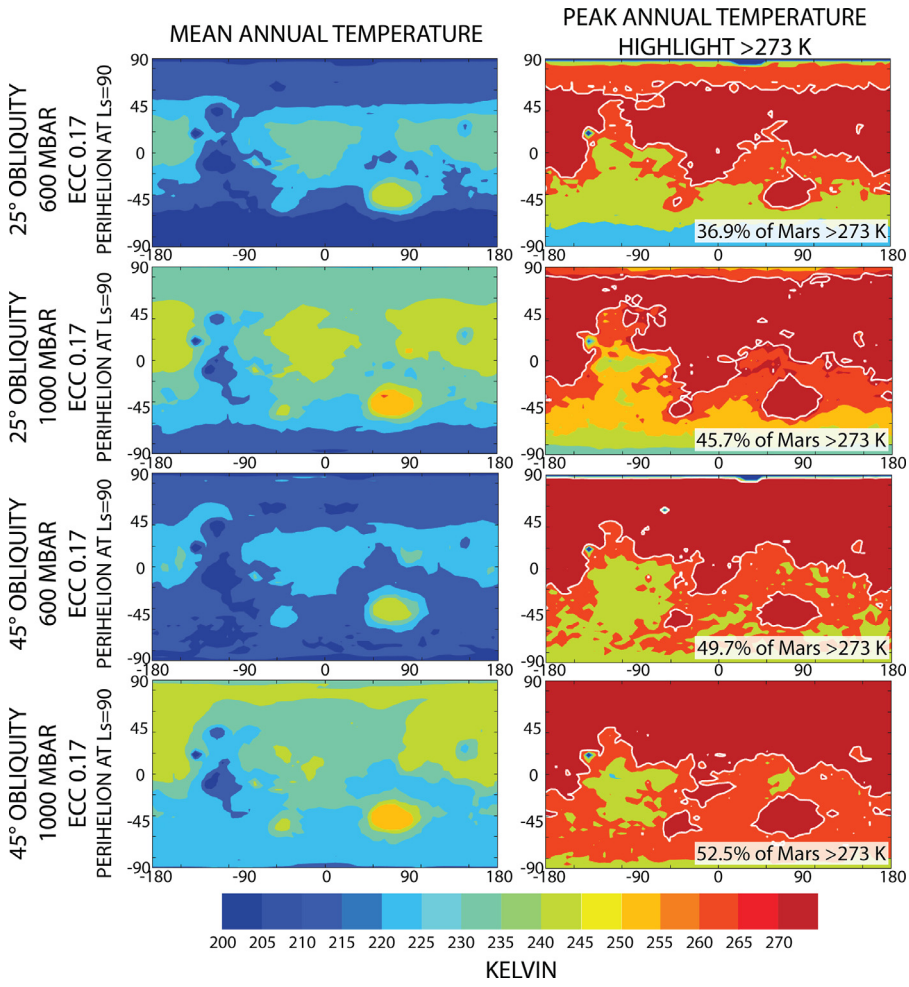

Fig. 3. Global maps of the mean (column A) and peak (maximum) (column B) annual temperature for a pure CO_2 atmosphere and an orbit with eccentricity of 0.17, which is a statistical upper limit (20% probably of occurring in the past 5 billion years) for martian eccentricity during the Noachian (Laskar et al., 2004). Here we consider a longitude of perihelion of $L_s = 90$. Compare to Fig. 2 which shows the same maps for a circular orbit. The increased eccentricity results in longer and warmer summer seasons (specifically in the northern hemisphere during higher obliquity), producing larger regions of PAT > 273 K than for a circular orbit (Fig. 2) under similar spin-axis/orbital and pressure conditions.

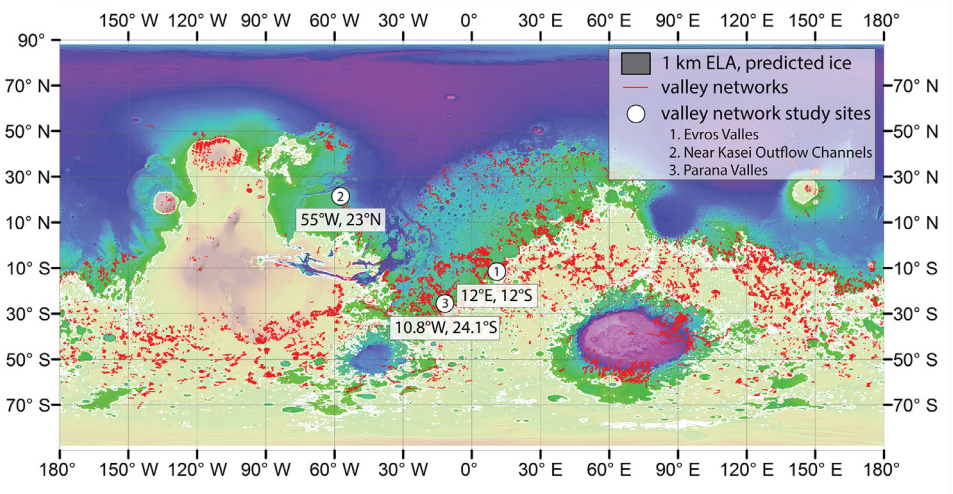

Fig. 4. The distribution of valley networks and the predicted distribution of snow and ice in the LNIH model. Valley network distribution map (red lines; Hynek et al., 2010) superposed on the predicted "Late Noachian Icy Highlands" ice distribution at 1 km ELA (equilibrium line altitude) (Head and Marchant, 2014). The locations of the three valley networks sites analyzed in this study are shown. Topography is MOLA data (brown is high, purple is low). (For interpretation of the references to color in this figure legend, the reader is referred to the web version of this article.)

0.17. These cases represent (1) both a low obliquity (25°) and the most probable average Noachian obliquity (45°, most likely obliquity is 41.8°; Laskar et al., 2004), (2) relatively low and high atmospheric pressure values (600 and 1000 mbar), and (3) the full range of probable eccentricity values (0 and 0.17). The model is run, with fixed conditions, for 10 years; all model data are taken from model year ten or higher to ensure equilibration of the model parameters utilized here. We utilize hourly data to ensure that we are capturing the warmest daily temperatures.

3.1. Pure CO_2 atmosphere

3.1.1. Mean annual temperatures (MAT) and peak annual temperatures (PAT)

The global distribution of MAT (globally averaging ~225 K) predicted by our GCM analyses is shown for 25° obliquity and 600 mbar (Fig. 2a-1). For the remainder of this discussion, we will refer to the column as its corresponding letter and the row as its corresponding number; for example, Fig. 2a-1 implies Fig. 2, column a, row 1), 25° obliquity and 1000 mbar (Fig. 2a-2), 45° obliquity and 600 mbar (Fig. 2a-3), and 45° obliquity and 1000 mbar (Fig. 2a-4) for a circular orbit and, similarly, repeated for the same spin-axis and atmospheric pressure conditions for the higher eccentricity value (eccentricity of 0.17; Fig. 3a-1–4 has perihelion at $L_s = 90$ or northern hemispheric summer, and Fig. 5a-1–4 has perihelion at $L_s = 270$ or southern hemispheric summer). Within this parameter space, the equilibrated ice distribution is that derived for a "Late Noachian Icy Highlands" scenario (Wordsworth et al., 2013, 2015) (Fig. 4). With global MAT (~225 K) far below (48 K) the 273 K melting point, we ask the question: Could PAT exceed 273 K in the warmest parts of the year, the melting point of pure water ice?

To evaluate this question and determine whether or not temperatures exceed 273 K at any point on Mars during the year, we produced PAT maps showing the peak annual temperature at every pixel across the globe for each of the four aforementioned studied cases (Figs. 2b-1–4, 3b-1–4, 5b-1–4). Our analysis shows that peak annual temperatures exceed 273 K somewhere on Mars during the year in all cases treated (600–1000 mbar, 25–55° obliquity, 0–0.17 eccentricity).

First, we consider the case of a circular orbit (eccentricity of 0, Fig. 2). How does PAT change with increasing CO_2 atmospheric pressure? As the amount of CO_2 in the atmosphere increases, the greenhouse effect becomes stronger and peak temperatures become more significant, increasing across the planet (compare Fig. 2b-1 and 2b-2). Also, as the total atmospheric pressure increases, the amplitude of the diurnal cycle decreases somewhat because the atmospheric heat capacity is larger. This mechanism acts to counteract the increased CO_2 greenhouse effect on the diurnal timescale, making it more difficult for temperatures under a thicker atmosphere to reach daytime conditions > 273 K for MAT < 273 K. However, the strengthened greenhouse effect is the more powerful mechanism at play under these spin-axis/orbital conditions and thus, the increased CO_2 atmospheric pressure corresponds to a global increase in both MAT and PAT. At 25° obliquity and 600/1000 mbar pressure (Fig. 2b-1, 2b-2), PAT > 273 K occurrences are concentrated mostly in the northern lowlands and the floors of the Hellas and Argyre impact basins due to the altitude dependence on temperature. Temperatures across the planet increase with increasing atmospheric pressure (1000 mbar) and, thus, the percentage of the planet with PAT > 273 K also increases (compare Fig. 2b-1 and 2b-2, regions outlined in white). For example, for 25° obliquity and 600 mbar conditions (Fig. 2b-1), ~22.8% of the planet has PAT > 273 K, but with increased atmospheric pressure (1000 mbar) (Fig. 2b-2), the percentage of the planet with PAT > 273 K increases to ~28.4%. This trend is illustrated in Fig. 2b, where all regions with PAT > 273 K are outlined in white. Comparison of the PAT distribution plots with a map of the predicted distribution of snow and ice in the LNIH model (Fig. 4) and the distribution of valley networks (Fig. 4) shows that a few areas with both snow and valley networks correspond to the regions of PAT that exceed 273 K (compare Figs. 2b-1–4 and 4).

Noteworthy is the fact that maximum temperatures (see PAT maps, Fig. 2b) in the northern lowlands are higher at higher obliquity due to the latitudinal effects of solar insolation with increasing obliquity. This is illustrated in Fig. 2b-1 (25° obliquity and 600 mbar CO_2 atmosphere) and Fig. 2b-3 (45° obliquity and 600 mbar CO_2 atmosphere). At lower (25°) obliquity, the highest maximum temperatures are located closer to the equator, while at higher (45°) obliquity, the highest maximum temperatures have shifted toward the poles. Although the results of our highest obliquity simulations (55°) are not shown in Fig. 2, the results are substantively the same as those of the 45° obliquity simulations, with maximum temperatures shifted slightly more towards the poles.

Next, we repeat our study for the case of a more eccentric orbit (Fig. 3, perihelion at $L_s = 90$; Fig. 5, perihelion at $L_s = 270$) (eccentricity of 0.17, upper limit of our analyzed eccentricity range because higher eccentricities have less than 20% probability of having occurred in the past 5 billion years; Laskar et al., 2004). This eccentricity range has not been studied in full detail previously, and thus our analysis provides important information about the influence of eccentricity on climate. For example, in a more eccentric orbit, the strength of the seasonal cycles increases and, depending on the perihelion conditions, one hemisphere will experience a warmer summer than in the circular orbit scenario. In other words, for simulations where perihelion occurs during southern hemispheric summer (longitude of perihelion of $L_s = 270$), summertime temperatures in the southern hemisphere are increased because the planet is closer to the Sun during the summer season and farther from the Sun during the winter season, as compared to a less eccentric, or circular, orbit. Thus, in the higher eccentricity scenario, peak summer temperatures increase and peak winter temperatures decrease for the hemisphere that experiences the summer season during perihelion. Understanding the consequences that variations in eccentricity have on MAT and PAT distributions is important for this study because increasing eccentricity increases peak summertime temperatures for the hemisphere that is in the summer season during perihelion, potentially permitting the production of more seasonal meltwater than in the circular orbit case. Additionally, the precession timescale is ~50 ky, significantly shorter than the estimated timescale for formation of simple valley networks (~10^8 years total; Hoke et al., 2011). To remedy this, we analyze two datasets of opposite perihelion to better understand the influence of eccentricity variation and analyze the dataset by assuming that both perihelion scenarios persist for approximately half of the duration of valley network formation. The two perihelion scenarios that we consider in this analysis are (1) perihelion at $L_s = 90$, or northern hemispheric summer, and (2) perihelion at $L_s = 270$, or southern hemispheric summer.

The overall temperature distribution patterns observed in the circular orbit case are also observed here for the more eccentric case (Fig. 3; northern hemispheric summer at perihelion). As obliquity increases from 25° to 45° (compare Fig. 3b-1 and 3b-3), PAT increase in the polar regions and decrease in the equatorial region (for example, compare Fig. 3a-2 and Fig. 3a-4). However, in the higher eccentricity scenario, the effects of thermal blanketing by higher atmospheric pressure appear to significantly decrease the amplitude of the diurnal cycle. Thus, in contrast to the circular orbit scenario, as atmospheric pressure increases from 600 to 1000 mbar (compare Fig. 3a-1 and 3a-2), although MAT across the globe increase by ~10 K,

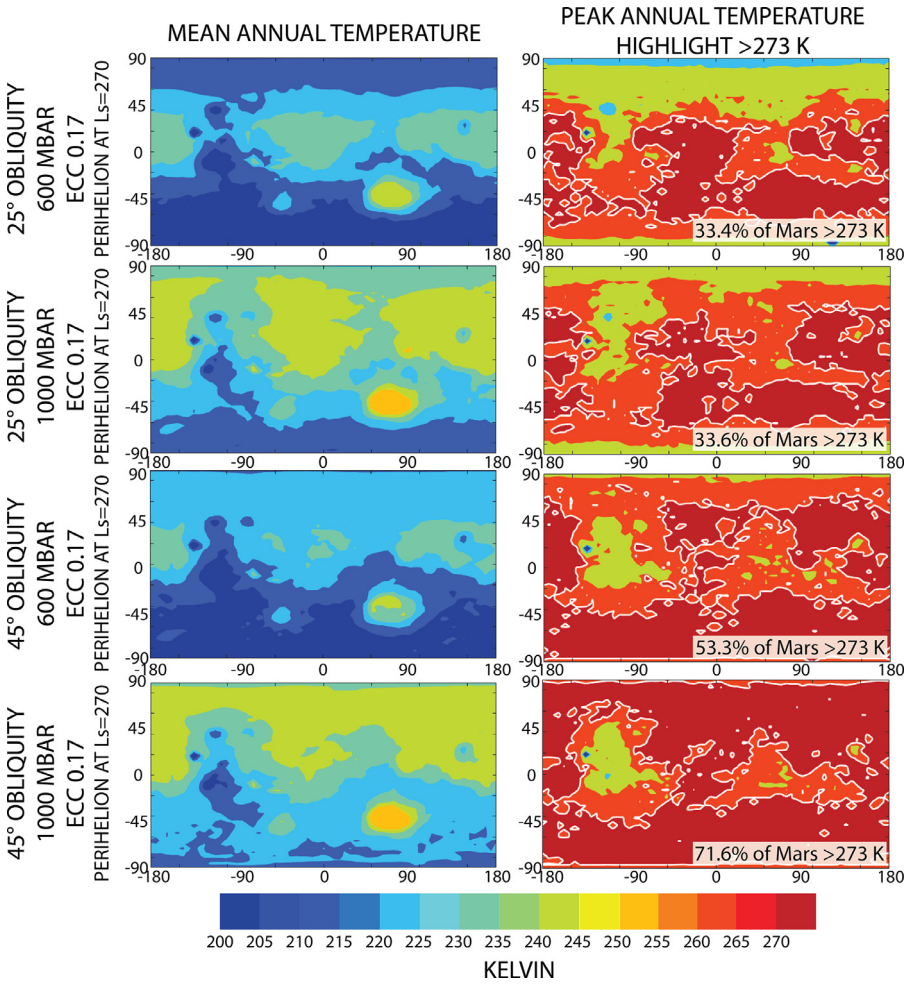

Fig. 5. Same as Fig. 3, except showing the reversed perihelion simulations (longitude of perihelion $L_s = 270$).

the area of the region with PAT > 273 K does not increase significantly (compare regions outlined in white in Fig. 3b-1 and 3b-2 or Fig. 3b-3 and 3b-4). For example, approximately the same percentage of the globe is characterized by PAT > 273 K at 45° obliquity and 600 mbar (Fig. 3b-3) and 45° obliquity and 1000 mbar (Fig. 3b-4). In a manner similar to circular orbit conditions, under these spin-axis/orbital conditions, PAT > 273 K occurs both in the northern hemisphere and in equatorial regions where valley networks are abundant (see Fig. 3b and compare to Fig. 4). PAT in the southern hemisphere are lower than PAT in the northern hemisphere because of the altitude dependence of temperature and because the longitude of perihelion ($L_s = 90$) is such that the northern hemisphere experiences summer at perihelion and the southern hemisphere experiences summer at aphelion.

In simulations where the perihelion occurs at $L_s = 270$ (Fig. 5; southern hemispheric summer at perihelion), we observe similar patterns to those observed in the previous simulations. As a consequence of the perihelion conditions, PAT in the southern hemisphere are warmer than in both the circular orbit and the reversed perihelion simulations; in significant portions of the southern hemisphere PAT exceed 273 K (Fig. 5b). This perihelion scenario (longitude of perihelion of $L_s = 270$) is critical to summertime melting because southern hemispheric summer occurs at perihelion; since a significant portion of the Noachian ice sheet was likely distributed in the southern hemisphere, this perihelion scenario can produce significantly more meltwater than the perihelion scenario in which northern hemispheric summer occurs at perihelion.

Our initial study of temperature distributions suggests that increasing the eccentricity to 0.17 introduces significantly more seasonal warming (see Figs. 3 and 5) than for conditions of a circular orbit; the percentage of the planet with PAT > 273 K is greater than in the case of a circular orbit. For example, for the conditions of a 600 mbar CO_2 atmosphere and 25° obliquity, 22.8% of the planet experiences PAT > 273 K when considering a circular orbit, and up to 33.4% of the planet experiences PAT > 273 K when considering an orbit with eccentricity of 0.17 (for conditions of perihelion occurring during southern hemispheric summer). Additionally, variations in perihelion control where the meltwater will be concentrated, depending upon which hemisphere is experiencing the summer season when Mars approaches perihelion.

In summary, throughout the parameter space explored (atmospheric pressure, obliquity, eccentricity), PAT greater than or equal to 273 K (regions outlined in white in Figs. 2, 3, and 5) occur in the northern lowlands, topographic lows such as the floors of basins, and parts of the equatorial region, but equatorial temperatures > 273 K only partially spatially correlate with regions where valley networks are observed (Fig. 2b1–4, 3b1–4, 5b1–4; compare to Fig. 4). For the case of a circular orbit, as obliquity increases, the highest MAT and PAT begin to shift towards the pole and as atmospheric pressure increases, the greenhouse effect increases, thus increasing MAT and the percentage of the globe with PAT > 273 K.

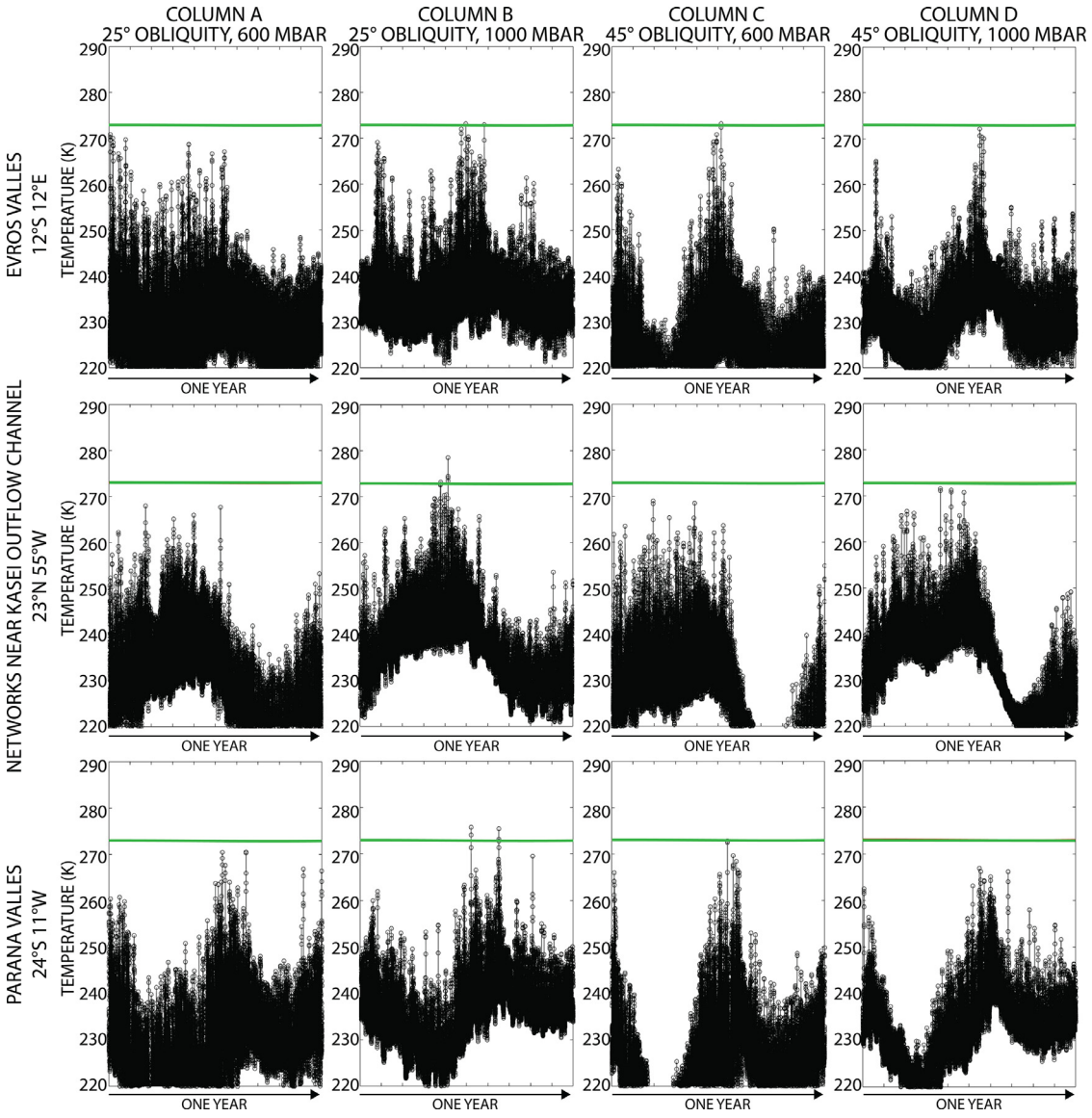

Fig. 6. Temperature time series (one martian year duration, beginning at $L_s = 0$) for all conditions studied in Fig. 2 (circular orbit) at three different valley network systems distributed at different latitudes and longitudes (see Fig. 4 for locations). Column A is 25° obliquity and 600 mbar CO_2. Column B is 25° obliquity and 1000 mbar CO_2. Column C is 45° obliquity and 600 mbar CO_2. Column D is 45° obliquity and 1000 mbar CO_2. Valley network locations are 1 (top) Evros Valles (12°S, 12°E), 2 (middle) the valley networks near the Kasei Outflow Channels (23°N, 55°W), and 3 (bottom) Parana Valles (24.1°S, 10.8°W). Horizontal lines at 273 K provide a reference to show how close PAT approach the melting point of water. Green lines highlight examples when temperatures approach (temperatures exceed 265 K at some point during the year) or are above 273 K for at least one data point during the year. Red lines indicate when temperatures approach, but do not exceed 273 K (temperatures are consistently below 265 K). Note that all horizontal lines are green. (For interpretation of the references to color in this figure legend, the reader is referred to the web version of this article.)

In other words, lower obliquity conditions permit warmer temperatures in the equatorial region (where valley networks are most abundant), and higher pressure increases temperature globally, increasing the percentage of the planet with PAT above the melting point of water. Based on these results and thermal considerations for the production of meltwater, we predict that the optimal spin-axis/orbital conditions to produce equatorial melting are relatively low obliquity and elevated atmospheric pressure. For the case of a more eccentric orbit (eccentricity 0.17), the same obliquity effects are observed, but as atmospheric pressure increases, increasing the greenhouse effect, the increased thermal blanketing significantly decreases the diurnal cycle and, although MAT increases on a global scale, the percentage of the globe with PAT > 273 K does not significantly increase. Higher eccentricity increases the possibility of seasonal summertime melting in regions with abundant valley networks for conditions characterized by perihelion at southern hemispheric summer, because significant meltwater can be produced in the southern hemisphere. Thus, higher eccentricity conditions are more optimal for the production of meltwater in regions with abundant valley networks than circular orbit conditions.

3.1.2. Valley network analysis: temperature time series

Our exploration of parameter space has shown that PAT in excess of 273 K, and thus areas conducive to melting of surface snow and ice, can occur in equatorial regions where valley networks are observed (Fig. 4). Uncertain, however, is whether these temperatures will persist long enough to create significant melting and subsequent surface runoff. In order to produce the maximum temperature plots shown in Fig. 2b (and Figs. 3b and 5b for eccentricity of 0.17), we sampled the maximum temperature reached throughout the year at each lat/lon model grid point. We ask the question: Do temperatures > 273 K occur at more than one data

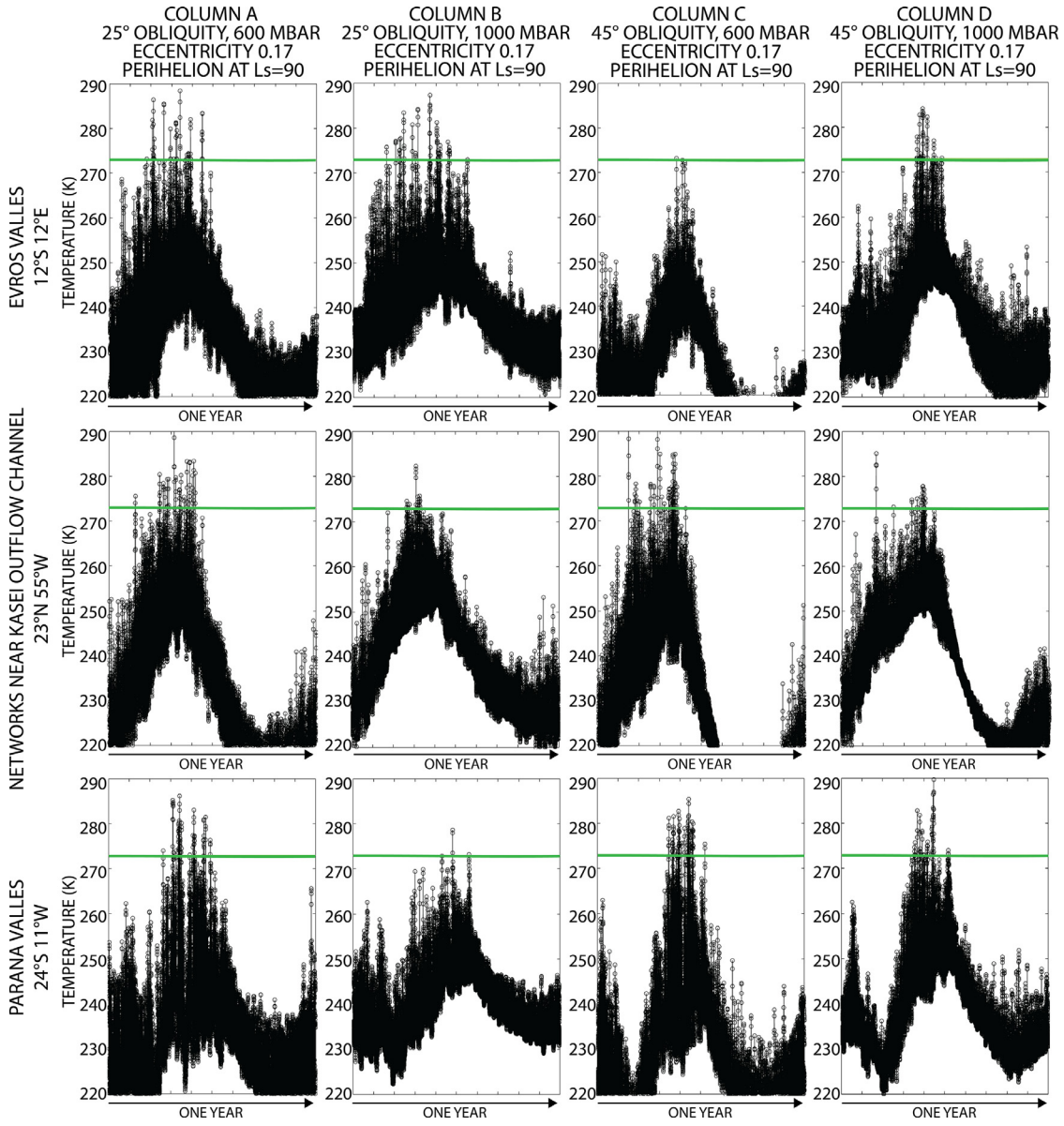

Fig. 7. Temperature time series (one martian year duration) for all conditions studied in Fig. 3 (orbital eccentricity of 0.17, longitude of perihelion of $L_s = 90$) at three different valley network systems distributed at different latitudes and longitudes (see Fig. 4 for locations). Column A is 25° obliquity and 600 mbar CO_2. Column B is 25° obliquity and 1000 mbar CO_2. Column C is 45° obliquity and 600 mbar CO_2. Column D is 45° obliquity and 1000 mbar CO_2. Valley network locations are 1 (top) Evros Valles (12°S, 12°E), 2 (middle) the valley networks near the Kasei Outflow Channels (23°N, 55°W), and 3 (bottom) Parana Valles (24.1°S, 10.8°W). Horizontal lines at 273 K provide a reference to show how close PAT approach the melting point of water. Green lines highlight examples when temperatures approach (temperatures exceed 265 K at some point during the year) or are above 273 K for at least one data point during the year. Red lines indicate when temperatures approach, but do not exceed 273 K (temperatures are consistently below 265 K). Note that all horizontal lines are green. (For interpretation of the references to color in this figure legend, the reader is referred to the web version of this article.)

point (on the time domain; e.g. one data point is collected every model hour) during the martian year, suggesting that temperatures > 273 K persist for more than just the warmest hour of the warmest day in the summer season? In order to assess the duration of temperatures > 273 K at each lat/lon model grid point, we collected model data 24 times per martian day (hourly), 16,056 times per martian year. While the PAT maps represent only one data point, it is possible that, at locations where PAT > 273 K (Figs. 2, 3, 5), temperatures > 273 K may occur at more than one data point during the year, suggesting a longer duration of conditions suitable to melting of surface ice. In fact, such conditions would be required to produce sufficient melting and runoff to form the observed fluvial and lacustrine features. To determine whether the PAT values at each lat/lon grid point correspond to a single data point, a few data points, or a summer average, we produced temperature time series for one model martian year. We do this for all the previously described obliquity, pressure, and eccentricity conditions (Fig. 6, circular; Fig. 7, eccentricity 0.17 with perihelion at $L_s = 90$; Fig. 8, eccentricity of 0.17 with perihelion at $L_s = 270$).

For this part of the analysis, we focus on three specific valley network systems (locations shown in Fig. 4): (1) Evros Valles (12°S, 12°E), (2) valley networks near the Kasei outflow channels (referred to as the Kasei site; 23°N, 55°W), and (3) Parana Valles (24.1°S, 10.8°W). We chose examples at these different longitudes and latitudes in order to obtain a global sampling of regions where valley networks are abundant and to assess the percentage of the year that these different areas experience temperatures in excess of 273 K. In the MDV, for example, temperatures

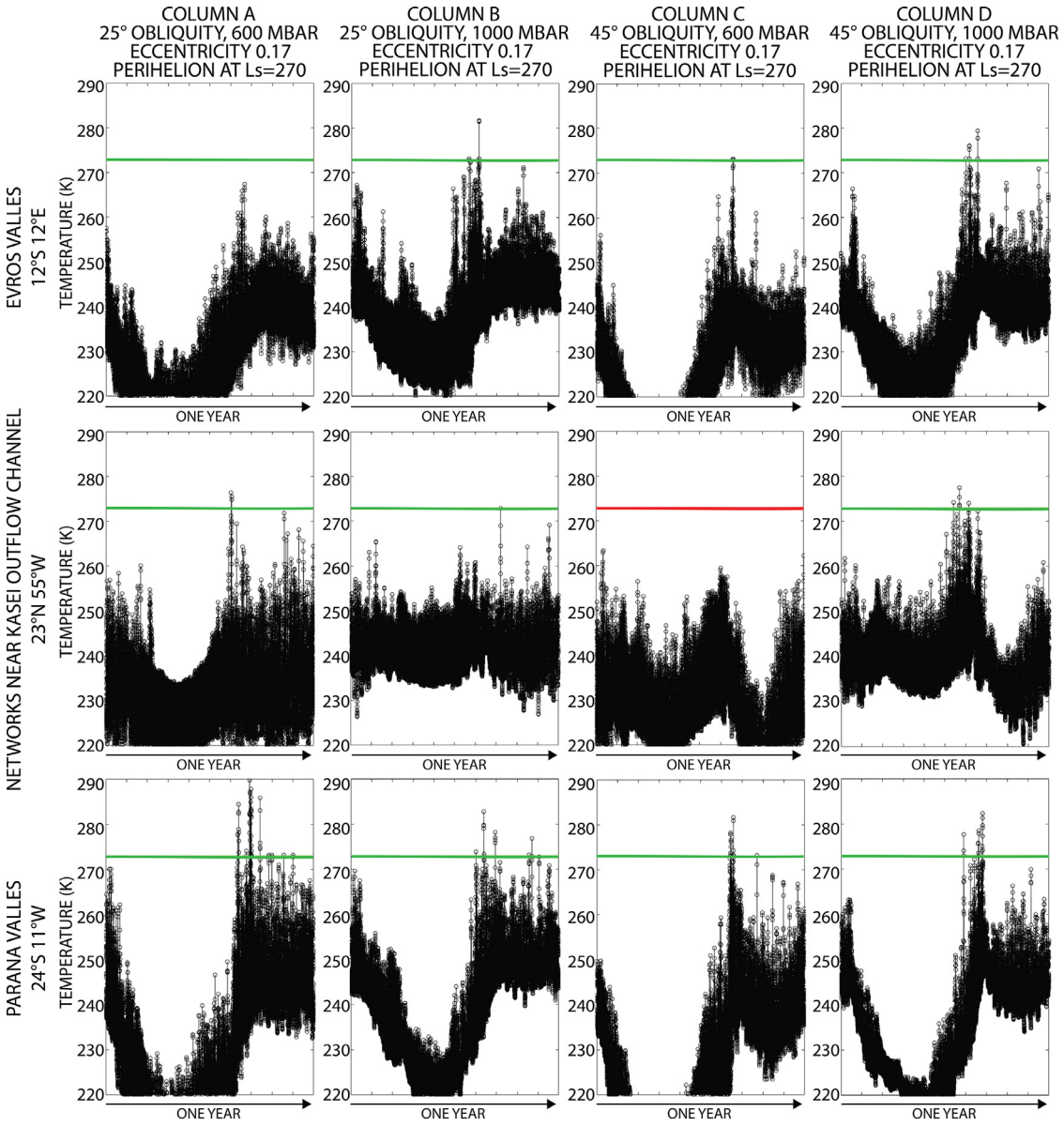

Fig. 8. Temperature time series (one martian year duration) for all conditions studied in Fig. 5 (orbital eccentricity of 0.17, longitude of perihelion of $L_s = 270$). Note that, under some conditions at some locations, horizontal lines are red; temperatures are consistently below 265 K. (For interpretation of the references to color in this figure legend, the reader is referred to the web version of this article.)

above 273 K are achieved during only a few percent of the year, and yet fluvial features similar to those on Mars are observed to form and persist from year to year (Head and Marchant, 2014). We have analyzed Long Term Ecological Research (LTER) climate monitoring data for Lake Hoare, in Taylor Valley of the MDV (https://lternet.edu/sites/mcm), and find that (1) under average annual conditions—where both MAT and PAT are comparable to adjacent years—approximately 5–7% of the year is characterized by surface temperatures > 273 K; and (2) under warmer than average annual conditions—where both MAT and PAT are slightly higher than adjacent years—approximately 11% of the year is characterized by surface temperatures greater than 273 K. Although these ambient Antarctic conditions are of course not directly comparable to Noachian "cold and icy" conditions because the MDV climate scenario is driven by seasonal temperature variation and lacks significant diurnal variation, we use the fact that transient seasonal warming for a minimum of ~5–7% of the year is a duration that permits local seasonal melting of accumulated snow and ice and leads to transient fluvial and lacustrine activity in the MDV as a broad interpretive guideline for this study.

First, we focus on the case of a circular orbit (Fig. 2). Fig. 6 shows temperature time series at the three valley network sample locations, and encompassing one martian year, for the conditions shown in Fig. 2. In all figures representing the results of our valley network analysis (Fig. 6 corresponds to circular orbit conditions; Figs. 7 and 8 correspond to eccentricity of 0.17 with perihelion at $L_s = 90$ and $L_s = 270$, respectively), the horizontal lines show the location of the 273 K ice melting temperature; the horizontal lines are green when temperatures approach the melting point of water (temperatures exceed 265 K at some point during the year) and red when temperatures do not approach the melting point of water (temperatures never exceed 265 K). The green lines at 273K in all panels in Fig. 6 show that temperatures approach the melting point at all locations under all spin-axis conditions (temperatures exceed 265 K at some point during the year). However, these time series plots (Fig. 6) show that, at these three valley network

locations, melting conditions (273 K) are either never reached or, if they are reached, only last for a few data points per year. Because we utilize hourly data in this analysis, it is possible that the data points above 273 K represent peak day time conditions from the warmest days in the summer season. Thus, with only a few data points above 273 K, we conclude that these conditions permit only one or a few days per year where melting conditions are reached during peak day time conditions. When we compare this to the conditions required to form similar fluvial and lacustrine features in the MDV, such a short annual period of melting would likely be insufficient to form the observed martian fluvial and lacustrine surface features.

Under some conditions, however, such as 25° obliquity and a 1000 mbar CO_2 atmosphere (Fig. 6), the valley networks near the Kasei site hover just below 273 K for a more significant portion of the year (for example, 22 days have maximum temperatures greater than or equal to 265 K, approximately 3.3% of the year). Seasonal variation in temperature in the MDV, where fluvial features are present, imply that, while melting conditions are not persistent, being close to the melting point for approximately one season could allow for fluvial features to form or persist under specific conditions (Head and Marchant, 2014). However, this scenario requires one season, or ~25% of the year, to have temperatures close to the melting point (in other words, summer PST ~273 K), which is much more than the model simulations suggest for these early martian spin-axis/orbital and pressure conditions. Therefore, although temperatures can be close to 273 K for multiple days in the summer season, we conclude that the duration is still not sufficient to sustain fluvial and lacustrine features under conditions of a pure CO_2 atmosphere and a circular orbit.

Next, we focus on the case of a more eccentric orbit, with eccentricity of 0.17 (Fig. 7, perihelion occurs at $L_s = 90$; Fig. 8, perihelion occurs at $L_s = 270$). As previously mentioned, the increased eccentricity leads to more extreme seasonal cycles, and thus to increased PAT due to warmer summertime conditions. This is expressed in the form of (1) a higher percentage of the planet characterized by PAT > 273 K, and (2) a difference in number of days in which temperatures rise above 273 K at the valley network locations studied. Locations that never reach 273 K in the circular orbit are now characterized by temperatures greater than 273 K, sometimes for multiple days depending on which hemisphere experiences summertime during perihelion (Figs. 7 and 8). For example, the Kasei site experiences less time above freezing than Parana Valles for conditions of southern hemispheric summer at perihelion (Fig. 8). A significantly higher percentage of the year is characterized by temperatures > 273 K at the valley network locations for the case of a more eccentric orbit, with values more similar to what is observed in the MDV (maximum 25 days with PAT > 273 K at the Kasei site (~4% of the year), maximum 30 days with PAT > 273 K at Parana Valles (~4.5% of the year), and maximum 22 days with PAT > 273 K at Evros Valles (~3% of the year); the maximum values are taken as the maximum value from either perihelion scenario). Thus, the results from the simulations with eccentricity of 0.17 are more promising for the production of significant summertime melting than that of a circular orbit and we explore these conditions further in a later section.

There are some conditions which result in a greater portion of the year with temperatures temporarily stabilized just below 273 K, in a manner similar to the case of a circular orbit. For example, at 25° obliquity and a 600 mbar CO_2 atmosphere with eccentricity of 0.17 and perihelion at $L_s = 90$, Parana Valles experiences PDT > 265 K for ~71 days (approximately 11% of the year). Under these same conditions, Evros Valles experiences PDT > 265 K for ~69 days (approximately 10% of the year) and the valley networks near the Kasei site experience PDT > 265 K for ~88 days (approximately 13% of the year). Thus, a significantly higher percentage of the summer season is characterized by temperatures that approach 273 K for increased eccentricity conditions. Although these conditions persist for a period much less than one season and there is likely to be significantly more diurnal temperature variation than observed during the summer season in the MDV, we consider that increased eccentricity conditions warrant further consideration when considering seasonal summertime melting (Head and Marchant, 2014).

In conclusion, when considering an eccentric orbit (0.17), the magnitude of the seasonal cycle is enhanced and significant seasonal melting can ensue, producing a number of days with PAT > 273 K at different valley networks that is comparable to what is observed in the MDV. However, when considering a circular orbit, although a "cold and icy" early Mars can have PAT > 273 K, such conditions appear to be of very short duration in the equatorial region and, in some cases, do not occur at certain valley network locations at all. Nonetheless, mean seasonal temperatures (MST) can hover below, but near 273 K. Based on the fact that fluvial and lacustrine features form in the slightly warmer MDV climate and in attempt to estimate atmospheric and spin-axis conditions where significant melting can occur in the equatorial region for a circular or low eccentricity (significantly less than 0.17) orbit, we raise the question: Could the addition of small amounts of greenhouse gases raise temperatures above 273 K for a period of time during the year sufficient to produce enough melt to erode the valley networks, when repeated over many years, while maintaining MAT < 273 K? We do not aim to reproduce the MDV climate exactly because of differences in seasonal and diurnal solar cycles, but attempt to reproduce the MDV seasonal melting effect by considering a climate that is characterized by MAT > 225 K but still <273 K. We speculate that, because PAT and seasonal temperatures in the "cold and icy" model (MAT ~225K) can approach 273 K, the observed fluvial and lacustrine features might be caused by the addition of small amounts of greenhouse gases in the atmosphere to produce temperature conditions suitable to melting for a few percent of the year, similar to what is observed in the MDV (e.g. Head and Marchant, 2014).

3.2. Addition of gray gas

There is still no consensus on the most likely combination of greenhouse gases that would serve to force a continuous overall "warm and wet" climate, characterized by MAT ~273 K. Previous studies have considered the warming effects of H_2O (e.g. Forget et al., 2013), CO_2 (e.g. Forget et al., 2013; Wordsworth et al., 2013), NH_3 (Kasting et al., 1992; Kuhn and Atreya, 1979; Sagan and Chyba, 1997; Wolf and Toon, 2010), CH_4 (e.g. Wordsworth et al., 2017), H_2S (Johnson et al., 2008), and SO_2 (Johnson et al., 2008). Currently, it appears that given reasonable source and sink constraints for these gases, permanent (>1,000,000 years) increases of MAT above 273 K are not possible, although extended periods of enhanced warming by their intermittent release may have occurred. Here, however, we explore whether the addition of greenhouse gases other than CO_2 into the atmosphere can increase the overall temperature slightly and, despite MAT still being much lower than 273 K, produce transient seasonal conditions suitable to melting in the equatorial region when considering a circular orbit, which we have shown cannot be done in an ambient CO_2 atmosphere. In lieu of knowledge of specific greenhouse gas species and quantities that might have been available in the late Noachian, and in order to cover a range of possibilities, we introduce a gray gas absorption into the model. A gray gas absorbs evenly across the spectrum at a defined absorption coefficient, κ. The addition of gray gas permits us to introduce a small amount of greenhouse warming, increasing overall temperatures by a few Kelvin, without

forcing the planet into a condition in which MAT is >273 K and a "warm and wet" climate state might result.

We focus on the forcing of moderate greenhouse warming in a "cold and icy" climate and on the possibility that moderate warming could be sufficient to permit seasonal melting and valley network formation without transitioning to a "warm and wet" climate. To accomplish this, we chose a relatively low value for the gray gas absorption coefficient, $\kappa = 2.5 \times 10^{-5}$ $m^2 kg^{-1}$, corresponding to an overall increase in globally averaged MAT of ~18K. We have chosen our gray gas absorption coefficient based on the analyses of Scanlon et al. (2016) and Fastook and Head (2015). Scanlon et al. (2016) analyzed the distribution and rates of snowfall, rainfall, and runoff, for a variety of different climate scenarios ranging from a typical "cold and icy" climate to a typical "warm and wet" climate. For this analysis, we have chosen to use the lowest absorption coefficient utilized by Scanlon et al. (2016), which represents the coldest (but still slightly warmed from the nominal "cold and icy" conditions) climate analyzed in their study. We choose to reproduce this climate scenario to emphasize the role of seasonal variability in predominantly "cold and icy" climates and to compare the implications of our results with the results from this previous study (Scanlon et al., 2016). Additionally, Fastook and Head (2015) estimate that a warming of at least ~18 K is necessary to produce significant meltwater under Noachian Mars conditions (they do not consider a higher eccentricity orbit, as we have done here), and we are testing this hypothesis with the GCM.

3.2.1. Mean annual and peak temperatures

The mean and peak annual temperatures for the gray gas scenarios (Fig. 9) are plotted in the same manner as shown previously under the pure CO_2 atmosphere case (Figs. 2, 3, 5). We consider the same obliquity and pressure range and present results for a circular orbit. In general, the same trends are observed in the "extra greenhouse gas" warming case, but now include the addition of a greenhouse-forced overall increase in globally averaged MAT of ~18 K (Fig. 9a).

At 600 mbar, as obliquity increases from 25° to 45° (compare Fig. 9b-1 and 9b-3), the warmest PAT migrate further towards the poles, and the equatorial region experiences overall colder temperatures.

Differences in the temperature distribution are evident when focusing on the regions outlined in white (PAT > 273 K) in Fig. 9b-1 (obliquity 25°, 600 mbar) and Fig. 9b-3 (obliquity 45°, 600 mbar); these show warmer temperatures at the poles and colder temperatures in the equatorial regions at higher obliquity. Specifically, at 25° obliquity, almost half of the equatorial region experiences PAT > 273 K, while at 45° obliquity, much less of the equatorial region is characterized by PAT > 273 K. However, due to the common atmospheric pressure of 600 mbar, a similar percentage of the planet experiences PAT > 273 K in both the 25° and 45° obliquity cases (warmest peak temperature conditions are shifted to higher latitudes for increased obliquity), with average percentages of PAT > 273 K of ~52% and ~58%, respectively.

As atmospheric pressure increases, an overall increase in temperatures is noted, and thus, a larger portion of the planet is characterized by PAT > 273 K. For example, 25° obliquity and 600 mbar CO_2 atmospheric pressure conditions (Fig. 9b-1) correspond to PAT > 273 K for ~52% of the planet, while increased atmospheric pressure (1000 mbar; Fig. 9b-2) conditions correspond to PAT > 273 K for ~61% of the planet.

3.2.2. Valley network analysis: temperature time series

Having achieved warmer overall temperatures by artificially increasing the greenhouse effect with a modest gray gas component, we now return to the question of the duration of conditions suitable to induce melting. We address the question: Can slightly higher greenhouse-forced temperatures produce seasonal melting of sufficient magnitude and duration to account for valley network formation when considering a circular orbit? We return to the three specific valley network study regions (Fig. 4), Evros Valles (12°S, 12°E), the Kasei site (23°N, 55°W), and Parana Valles (24.1°S, 10.8°W), and repeat the temperature time series analysis previously described. The results of this analysis (Fig. 10) can be compared to the earlier time series results for the pure CO_2 atmosphere and circular orbit simulations (Fig. 6). In this warmer scenario, the temperature time series at the given valley network locations show a consistent overall increase of ~10–18 K, corresponding to the global increase observed in the MAT/PAT maps (Fig. 9; globally averaged increase of ~18 K) from the additional greenhouse warming. In most cases, specifically the Kasei site, this increase from modest greenhouse warming is sufficient to produce peak summertime temperature conditions that result in PDT > 273 K for a few percent of the year. As expected, low obliquity and high atmospheric pressure conditions (25°, 1000 mbar) (Fig. 10b) optimize the effect, and consistently produce the highest percentage of the year above 273 K. For example, at the valley networks near the Kasei site, PDT > 273 K occurs on ~34 days, or ~5% of the year (Fig. 10b-2). These conditions are comparable to the durations observed in the MDV at Lake Hoare (https://lternet.edu/sites/mcm). We thus conclude that temperatures > 273 K persist for a sufficient length of time to melt ice and produce surface runoff at this location. It is important to note, however, that even with the inclusion of gray gas-induced warming, low pressure conditions (e.g. 600 mbar CO_2 atmosphere) (Fig. 10a) do not produce PDT > 273 K for more than ~1–2% of the year at the Kasei site.

In general, it follows that at 45° obliquity, valley networks at mid-latitudes will experience higher temperatures or longer durations of melting conditions (Fig. 10c-2 and 10d-2) than those closer to the equator (Fig. 10c-1 and 10c-3; Fig. 10d-1 and 10d-3), as the higher obliquity forces the maximum solar insolation to migrate to mid-latitudes (Fig. 9b-3 and 9b-4). Additionally, due to the altitude dependence on temperature, the southern hemisphere will experience colder temperatures than the northern hemisphere when considering a circular orbit.

When considering higher obliquity conditions (45°), the two valley network locations in the southern hemisphere, Evros Valles and Parana Valles (Fig. 4), do not experience as much of the year above 273 K as those near the Kasei site (Fig. 10). However, the additional modest greenhouse warming still produces melting conditions for a few data points of the year (maximum 6 days with PDT > 273 K or ~1% of the year at Evros Valles; maximum 7 days or ~1% of the year at Parana Valles). MDV analogs (e.g. Head and Marchant, 2014) suggest that only a few percent of the year above the melting point of water are required to produce features similar to the martian valley networks and lakes, but these values are a few percent lower than what we observe at Lake Hoare (~5–7%). On the other hand, the percentage of the year exceeding freezing temperatures at the Kasei site is comparable to what is observed at Lake Hoare.

Melting conditions are being reached more frequently than in the simulations without additional greenhouse warming and percentages of the year with daytime temperatures exceeding freezing approached values observed in the MDV, which might be significant when repeated over many years.

In summary, we have forced modest greenhouse warming through the addition of a gray gas in order to increase global temperatures by ~18 K, still keeping an overall "cold and icy" climate with MAT ~243 K, significantly below 273 K. By repeating the same time series analysis and corresponding assessment of specific valley network locations (Fig. 4), we find that a small amount of greenhouse warming increases temperatures sufficiently to induce melting of snow and ice, and produces melt conditions potentially

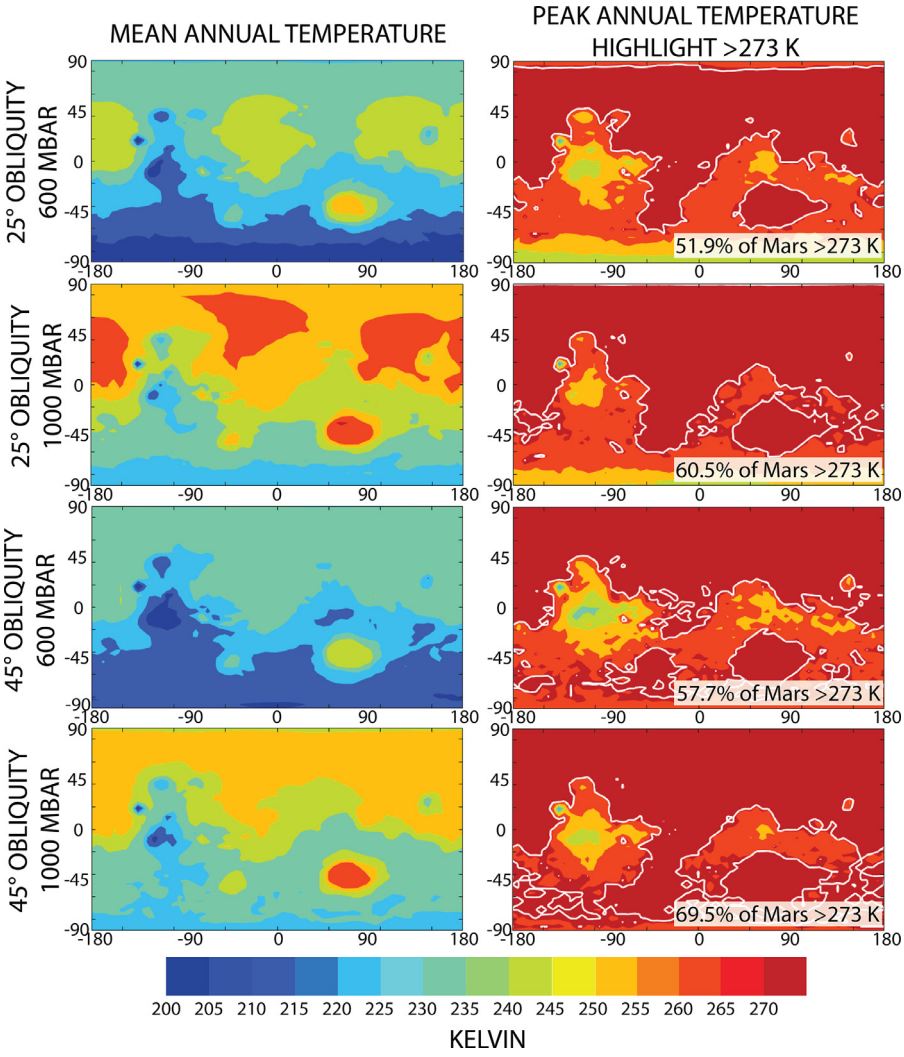

Fig. 9. Global maps of the mean (column A) and peak (maximum) (column B) annual temperature for a pure CO_2 atmosphere and a circular orbit, with the additions of a gray gas in the atmosphere to induce additional warming (absorption coefficient $\kappa = 2.5 \times 10^{-5}$ m^2 kg^{-1}; see text for details). Compare to Fig. 2 which portrays the same conditions without the addition of a gray gas. Shown are these mean and maximum values in conditions of different obliquity (rows 1 and 2 at 25° obliquity; rows 3 and 4 at 45° obliquity) and different atmospheric pressure (rows 1 and 3 at 600 mbar; rows 2 and 4 at 1000 mbar). All data shown here are taken from model year 10. Note the significantly larger area (column B, outlined in white) in which the PAT exceeds 273 K during the year. .

suitable for the formation of these valley networks if the process repeats for many years. All three regions studied (Fig. 4) are characterized by a low-to-modest percent of the year above 273 K, with the networks located in the northern hemisphere experiencing the longest duration of melt conditions (e.g. the Kasei site).

Recent work by Scanlon et al. (2016) studied the implications for snowmelt in a greenhouse-warmed "cold and icy" climate, varying the gray gas forced warming from the absorption coefficient we utilized in this study, $\kappa = 2.5 \times 10^{-5}$ m^2 kg^{-1}, to a warmer scenario, with $\kappa = 2 \times 10^{-4}$ m^2 kg^{-1}. For minimal additional warming, they conclude that snowmelt could explain runoff rates at some valley network locations, but not all. This is in agreement with our work, which suggests that the small amount of greenhouse forcing included here (the lowest amount of gray gas considered by Scanlon et al. (2016)) corresponds to a high enough percentage of the year above 273 K at the Kasei site (~5% of the year), and possibly insufficient percentages of the year at Evros Valles (~1% of the year) and Parana Valles (~1–4% of the year). Additionally, Scanlon et al. (2016) conclude that their warmest simulations ($\kappa = 2 \times 10^{-4}$ m^2 kg^{-1}; temperatures exceed 273 K by ~10–20 K for most of the year) produce too much continuous precipitation and snowmelt to form the observed valley networks. Thus, it is likely that the amount of greenhouse warming necessary to induce the appropriate scale of melting and erosion is less than the maximum considered by Scanlon et al. (2016), suggesting that MAT was likely to have been <273 K (without considering the influence of increased eccentricity). Although a plausible combination of greenhouse gases to produce a continuous "warm and wet" scenario has not been identified, a somewhat enhanced greenhouse effect can increase MAT above the "cold and icy" ~225 K MAT, producing slightly warmer conditions. We hypothesize that a combination of greenhouse gases could raise MAT to ~243 K, creating the conditions considered here and reproduced with gray gas ($\kappa = 2.5 \times 10^{-5}$ m^2 kg^{-1}). This scenario agrees with the conclusions reached by Scanlon et al. (2016): MAT > 273 K appears to produce too much precipitation and runoff; it appears that MAT < 273 K and >225 K are required for formation of the valley networks.

We are currently assessing additional methods to quantify more rigorously the necessary amount of additional warming and percentage of the year required to produce ice melting and water runoff to form the observed fluvial and lacustrine features. Next steps include (1) specific greenhouse gases: introducing and testing specific greenhouse gas combinations and quantities, within rea-

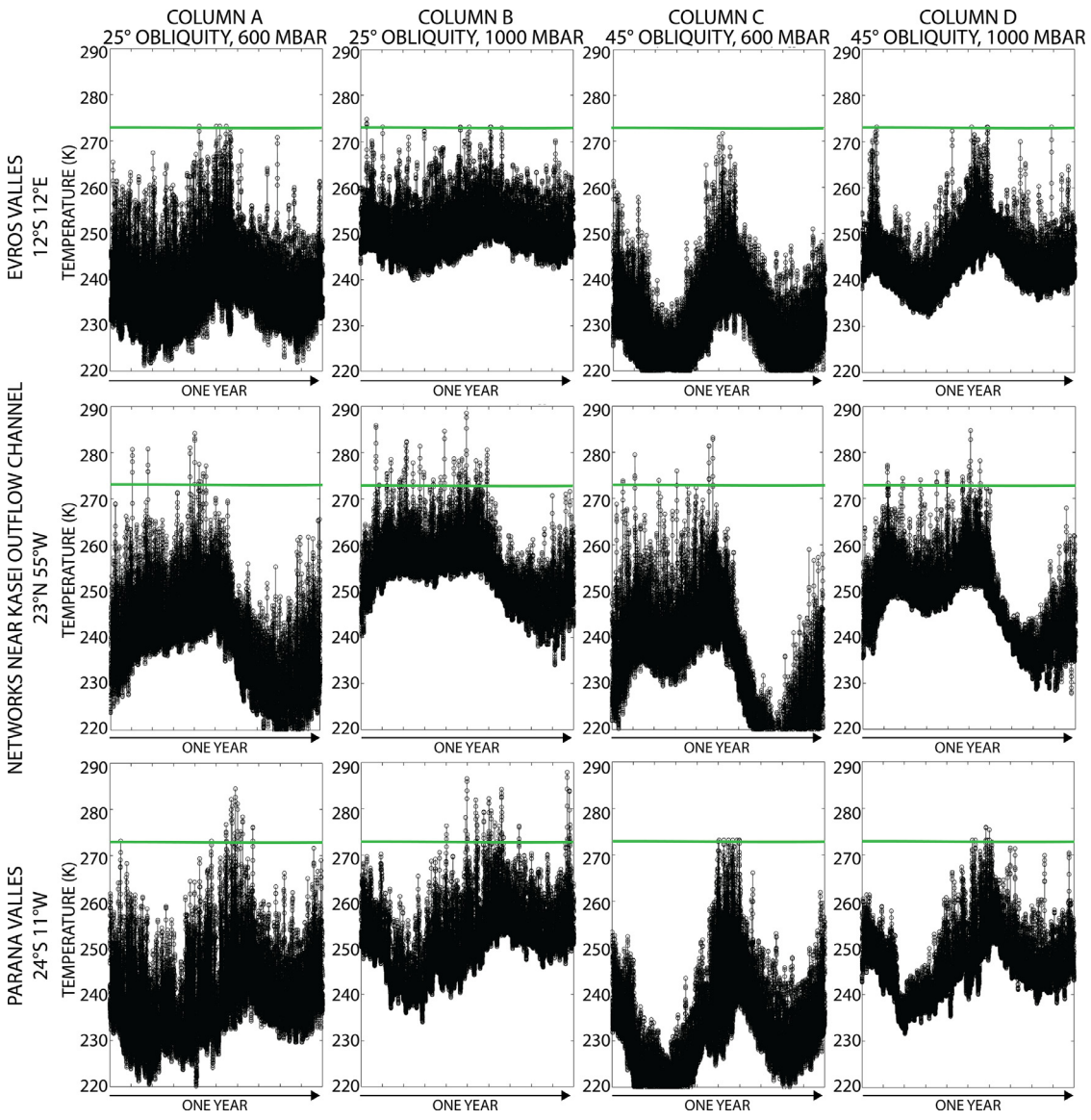

Fig. 10. Temperature time series (one martian year duration) for all conditions studied in Fig. 2 (circular orbit) but with the addition of a gray gas to induce warming (absorption coefficient $\kappa = 2.5 \times 10^{-5}$ m^2 kg^{-1}; see text for details). Data are for three different valley network systems distributed at different latitudes and longitudes (see Fig. 4 for locations). Column A is 25° obliquity and 600 mbar CO_2. Column B is 25° obliquity and 1000 mbar CO_2. Column C is 45° obliquity and 600 mbar CO_2. Column D is 45° obliquity and 1000 mbar CO_2. Valley network locations are 1 (top) Evros Valles (12°S, 12°E), 2 (middle) the valley networks near the Kasei Outflow Channels (23°N, 55°W), and 3 (bottom) Parana Valles (24.1°S, 10.8°W). Horizontal lines at 273 K provide a reference to show how close PAT approach the melting point of water. Green lines highlight examples when temperatures approach (temperatures exceed 265 K at some point during the year) or are above 273 K for at least one data point during the year. Red lines indicate when temperatures approach, but do not exceed 273 K (temperatures are consistently below 265 K). All horizontal lines approach or exceed 273 K. The greenhouse-forced overall increase in temperature of ~18 K permits all studied valley network locations to exceed 273 K for at least one data point per year (peak conditions for at least one day, annually). (For interpretation of the references to color in this figure legend, the reader is referred to the web version of this article.)

sonable source and sink constraints, to test more precisely what conditions might have been present and possibly responsible for forming the fluvial and lacustrine features under a Late Noachian "cold and icy" climate, and (2) influence of dust: further considering the effects of dust on the snow and ice, which will lower the albedo and allow the "dirty" ice layer to absorb more incoming shortwave radiation, permitting seasonal melting and possible surface runoff of the snow and ice at a lower temperature than is possible without dust (e.g. Wilson and Head, 2009; Kite et al., 2013; Clow, 1987).

3.3. Melt volumes

At this point in our study, we have determined that, with either a relatively high eccentricity (0.17) or a small amount of additional greenhouse warming, seasonal temperature variations can produce durations of melt conditions at specific valley networks comparable to what is observed in the MDV. Next, we constrain the predicted annual melt volumes further to determine whether this is a plausible mechanism for formation of the valley networks and lakes when repeated for many years. To do this, we have adopted and adapted the methods of a positive degree day (PDD) analysis, previously used for terrestrial snowmelt calculations (e.g. Huybrechts et al., 1991) and adapted for early Mars by Fastook and Head (2015). A PDD analysis uses temperature as a proxy for the thickness of ice melted in a single day; for a single day, the PDD value is identified as the average number of degrees above freezing. We follow these steps: (1) Determine the PDD values for each day in one model year at every lat/lon grid point. Then, we sum over the course of one year to produce an

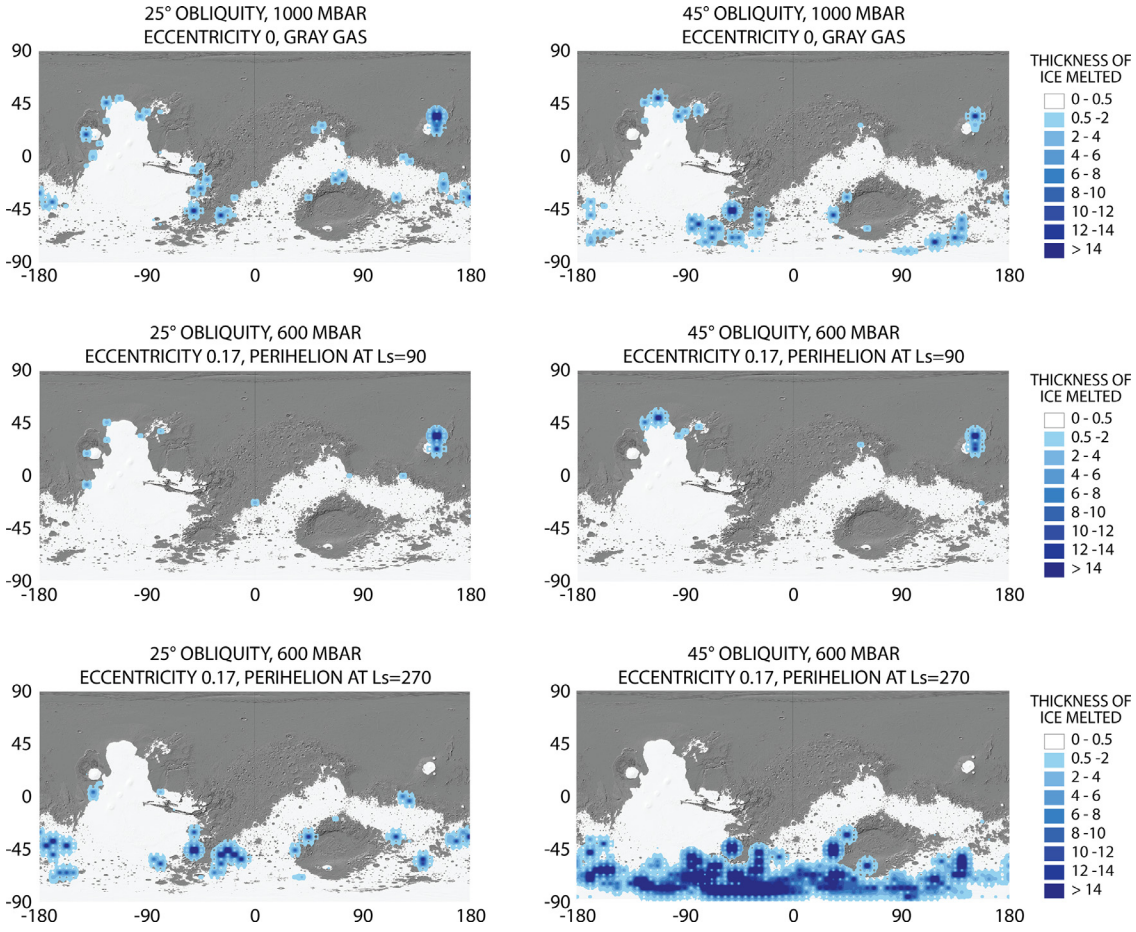

Fig. 11. Thickness of ice melted for varying spin-axis/orbital and pressure conditions (overlain on MOLA hillshade topography data; the predicted 1 km ELA ice sheet is shown as regions shaded in white and is used for calculations). The methods for performing this PDD calculation are described in the test. This figure illustrates that lower obliquity conditions are related to melting in the equatorial regions, where we observe valley networks, while higher obliquity conditions produce more melting poleward of 40°S. This confirms our previous conclusion that lower obliquity conditions are optimal for producing melt correlated with the valley networks. In cases where temperatures are > 273 K and valley networks are abundant but ice is not present, we consider that (1) there could be supply limitations preventing the current ice distribution to extend to this region and they could be produced at a later time when the ice distribution shifts due to spin-axis/orbital variations or (2) the actual ice distribution varied slightly from the utilized 1 km ELA ice distribution. If the former is the case, it is possible that ice limitations throughout the Noachian were a main driver for distribution of valley networks.

array of annual PDD values with one value per lat/lon grid point. (2) Compare the predicted 1 km equilibrium line altitude (ELA) (Head and Marchant, 2014) ice/snow distribution map with the map of annual PDD values, highlighting any areas where the annual PDD value is greater than 0 and ice/snow is present. If temperatures > 273 K are reached in areas where ice is present, melting can occur. (3) Next, we adopt the predicted rate for melting on early Mars of 1.08 mm/PDD (Fastook and Head, 2015). Fastook and Head (2015) determine this rate by scaling a terrestrial PDD melting rate, that has been confirmed to make close approximations for melting on terrestrial glaciers, to a Noachian Mars PDD melting rate by accounting for factors that affect the energy balance, including the decreased solar luminosity and the high snow-like surface albedo. At every lat/lon grid point where ice is present and the annual PDD value is greater than 0, we multiply the annual PDD value by 1.08 mm/PDD (Fastook and Head, 2015) to calculate the thickness of ice melted annually through this process at each lat/lon grid point (see Fig. 11). (4) Next, we determine the volume of meltwater produced by summing the total thickness of ice melted and then multiplying by the area where ice is present and the PDD value is greater than 0. A useful quantity for comparison between the annual volume of meltwater produced through this mechanism and the amount of water required to form the valley networks is the global equivalent layer (GEL) of meltwater produced through ice melting. To obtain this, we divide the volume of meltwater produced through this mechanism by the surface area of Mars. Rosenberg and Head (2015) suggest that 3–100 m GEL of water is required to form the valley networks. This is a predicted total amount of water and does not imply that all required water was on the surface at once. Thus, we can divide the total amount of water needed (3–100 m) by the amount produced annually through this mechanism to estimate how many years this process would be required to repeat to form the valley networks. Estimating the amount of annual meltwater produced and the required duration helps determine the viability of this process for forming the valley networks.

In previous sections, we have concluded that (1) a small amount of additional greenhouse warming is required to produce melt conditions (temperature > 273 K) at specific valley networks for a percentage of the year comparable to what is observed in the MDV, when considering a circular orbit, (2) higher atmospheric pressure increases temperatures globally and produces conditions more favorable to melting, however, for higher eccentricity simulations, increasing atmospheric pressure significantly decreases diurnal temperature variation, and (3) conditions of increased eccentricity can produce significantly more melting than circular orbit conditions, and possibly a volume of meltwater sufficient to form the valley networks when repeated for many years. For

these reasons, we have focused on four specific model simulations for the PDD analysis portion of our study: (1) 25° obliquity, 1000 mbar CO_2 atmosphere, circular orbit, and additional gray gas ($\kappa = 2.5 \times 10^{-5}$ m^2 kg^{-1}), (2) 45° obliquity, 1000 mbar CO_2 atmosphere, circular orbit, and additional gray gas, (3) 25° obliquity, 600 mbar CO_2 atmosphere, eccentricity of 0.17, and no gray gas, and (4) 45° obliquity, 600 mbar CO_2 atmosphere, eccentricity of 0.17, and no gray gas. The results are illustrated in Fig. 11. Fig. 11 confirms that melting occurs in the equatorial regions for lower obliquity conditions (e.g. 25°) and moves toward the pole as obliquity increases (e.g. 45°), and illustrates the thickness of ice melted during one comparison to the 1 km ELA predicted ice sheet. For low obliquity conditions, the melt distribution correlates with the edges of the ice sheet in the equatorial region and can produce a small quantity of liquid water runoff, annually, in regions where valley networks are abundant (see Fig. 4 for distribution of valley networks and predicted ice sheet). However, some valley networks are located in regions where melting is not expected to occur. If, however, the ice sheet retreated, potentially due to variations in spin-axis/orbital parameters, both the distribution of the ice sheet and the locations where meltwater is produced (at the edges of the ice sheet) would change.

For 25° obliquity, 1000 mbar CO_2 atmosphere, circular orbit, and additional gray gas, 2.10×10^{10} m^3 (1.45×10^{-4} m GEL) of meltwater is produced through this process annually. Thus, if 3–100 m GEL of water is required to produce sufficient meltwater to form the valley networks, this process would need to be repeated for 20,700–548,000 years. Estimated time durations to form simple valley networks suggest that individual valley network formation time spanned a minimum of 10^5–10^7 years, with total time to carve all valley networks constrained to be less than about 2×10^8 years (spanning the period of 3.6–3.8 Gya; Hoke et al., 2011). Thus, while specific valley networks suggest a formation timescale of 10^5–10^7 years, liquid water may have been intermittently flowing on the surface for a total of $\sim 10^8$ years, with formation of the valley networks being intermittent and formation of different valley network systems overlapping in time. In conjunction with the predicted distribution of melting (Fig. 11), the predicted duration implies that this mechanism could plausibly be responsible for the formation of many valley networks under low obliquity conditions.

For 45° obliquity, 1000 mbar CO_2 atmosphere, circular orbit, and additional gray gas, 1.58×10^{10} m^3 (1.28×10^{-4} m GEL) of meltwater is produced annually, implying that the process must repeat for 23,400–728,000 years to produce sufficient meltwater to form the valley networks. While this duration correlates with the predicted minimum time duration for formation of individual valley networks, the distribution of melting does not correlate well with the valley network distribution; melting is produced mostly poleward of 40° instead of in the equatorial region (Fig. 11). Thus, we suggest that the valley networks are unlikely to have formed through such seasonal melting processes under high obliquity conditions.

For 25° obliquity, 600 mbar CO_2 atmosphere, eccentricity of 0.17, and no gray gas, (1) for simulations with perihelion occurring at $L_s = 90$ (perihelion at northern hemispheric summer), 8.71×10^9 m^3 (6.01×10^{-5} m GEL) of meltwater is produced annually, implying that the process must repeat for 49,900–1,660,000 years to produce sufficient meltwater to form the valley networks; and (2) for simulations with perihelion occurring at $L_s = 270$, (reversing the perihelion conditions; perihelion at southern hemispheric summer), 2.68×10^{10} m^3 (1.97×10^{-4} m GEL) of meltwater is produced annually, implying that the process must repeat for 15,200–5,060,000 years to produce sufficient meltwater to form the valley networks. However, it is important to note that during conditions where perihelion occurs at $L_s = 90$, most meltwater is produced in the northern hemisphere near Tharsis, which is not a region with abundant valley networks. Thus, we consider that most of the meltwater to form the valley networks must be produced during conditions where perihelion occurs at $L_s = 270$. Because the perihelion will precess to the opposite value every ~50 ky, both perihelion situations would occur throughout $\sim 10^8$ years, the predicted duration of valley network formation. Thus, if we approximate that each of the perihelion situations occurred for half of the $\sim 10^8$ years of valley network formation, it should take 32,450–1,083,000 consecutive years to form the valley networks. However, as previously mentioned, meltwater is only produced in regions with abundant valley networks approximately half of the time (when perihelion occurs at $L_s = 270$), suggesting that this estimate is a minimum and it could take up to twice as long (~2,166,000 years) to produce the necessary amount of meltwater in regions where valley networks are abundant. In a manner similar to the scenario of a circular orbit with the same obliquity condition (25°) and additional greenhouse warming, the predicted distribution of meltwater suggests that these spin-axis/orbital conditions could reasonably have been characteristic of the values that were typical during the time of valley network formation (Fig. 11). The predicted timescale for valley network formation is shorter under the conditions of a circular orbit with gray gas, although both result in timescales within the range predicted by Hoke et al. (2011).

For 45° obliquity, 600 mbar CO_2 atmosphere, eccentricity of 0.17, and no gray gas, (1) for simulations with perihelion occurring at $L_s = 90$ (perihelion at northern hemispheric summer), 8.22×10^9 m^3 (5.68×10^{-5} m GEL) of meltwater is produced annually, implying that the process must repeat for 52,900–1,760,000 years to produce sufficient meltwater to form the valley networks; and (2) for simulations with perihelion occurring at $L_s = 270$ (reversing the perihelion conditions; perihelion at southern hemispheric summer), 1.19×10^{11} m^3 (8.25×10^{-4} m GEL) of meltwater is produced annually; implying that the process must repeat for 3,640–121,000 years to produce sufficient meltwater to form the valley networks. In a manner similar to the previous scenario, (1) meltwater produced during the conditions of perihelion at $L_s = 90$ occurs mostly at the edges of the ice sheet near Tharsis, not in equatorial regions where valley networks are abundant, suggesting that most of the meltwater that contributes to valley network formation is produced during conditions of perihelion at $L_s = 270$, and (2) because the orbit is non-circular, both perihelion scenarios would occur during the duration of valley network formation, suggesting a period of approximately 28,270–940,500 consecutive years is required to produce sufficient meltwater to form the valley networks under these spin-axis/orbital conditions. However, as previously mentioned, meltwater is not always produced in regions with abundant valley networks (e.g. when perihelion occurs at $L_s = 90$; Fig. 11), suggesting that this estimate is a minimum. Additionally, although the duration required to produce sufficient meltwater to incise the valley networks agrees with the predicted timescale for formation of valley networks (Hoke et al., 2011), similar to the scenario of a circular orbit with the same obliquity condition (45°) and additional greenhouse warming, the high obliquity condition causes the strongest incident solar radiation to be focused at higher latitudes during the summer season when most melting occurs, producing meltwater at higher latitudes, instead of in the equatorial region where valley networks are most abundant. For this reason, we conclude that lower obliquity conditions are more suitable to forming the observed valley networks.

Although not illustrated in Fig. 11, for optimal circular orbit conditions (25° obliquity, 1000 mbar CO_2 atmosphere) with no additional greenhouse warming (MAT ~225 K), only 1.83×10^8 m^3 (1.26×10^{-6} m GEL) of meltwater is produced annually and the process would need to repeat for 2,370,000–79,100,000 years to produce sufficient meltwater to form the valley networks.

Although this duration overlaps with the predicted duration for valley network formation (~10^8 years), it also extends outside of the predicted range for individual valley network formation (10^5–10^7 years), reinforcing the idea that additional greenhouse warming may be required for this process to be capable of forming the valley networks under circular orbit conditions. It is important to reiterate that higher eccentricity conditions are more favorable to the formation of the valley networks without additional greenhouse warming than circular orbit conditions, suggesting that eccentricity may have been an important factor in the early martian climate for seasonal melting under ambient "cold and icy" conditions (MAT ~225 K).

To conclude, the calculations undertaken here imply that the peak seasonal melting process could be responsible for forming the valley networks. Optimal spin-axis/orbital and atmospheric conditions for valley network formation are either (1) low obliquity (25°), high atmospheric pressure (1000 mbar), a circular orbit, and a small amount of additional greenhouse warming (gray gas, $\kappa = 2.5 \times 10^{-5}$ m^2 kg^{-1}; ~18 K global increase), or (2) low obliquity (25°), relatively lower atmospheric pressure (600 mbar), eccentricity of 0.17, and no additional greenhouse warming. Conditions of low obliquity (25°), high atmospheric pressure (1000 mbar), a circular orbit, and no additional greenhouse warming also produce the required quantity of meltwater in regions where valley networks are abundant. However, the duration required to produce this quantity of meltwater extends outside of the range of the predicted formation timescale for individual valley networks, suggesting that additional greenhouse warming or higher eccentricity may have been required for valley network formation in this climate scenario. Additionally, higher obliquity conditions focus the production of meltwater to higher latitude regions, not in the equatorial region where valley networks are abundant; this suggests that higher obliquity conditions are not optimal for valley network formation in a "cold and icy" climate. Thus, it is possible that the valley networks could have formed through seasonal melting under a "cold and icy" climate under conditions (1) with MAT ~243 K, or (2) of higher eccentricity (0.17). "Warm and wet" conditions and external forcing, such as impact cratering and volcanism, may not be required for valley network formation if there is either ~18 K additional greenhouse warming or significant periods of higher eccentricity.

3.3.1. Consideration of runoff rates

Based on the geomorphology of different valley network systems, Hoke et al. (2011) estimated necessary runoff rates for formation of the valley networks through intermittent runoff, finding that required rates are between mm/day and cm/day.

3.3.2. Consideration of runoff rates: MAT ~243 K, circular orbit, climate scenario

Based on our results (Fig. 11), melting has a maximum of ~20 mm/year for a given location on the globe when considering a circular orbit and additional greenhouse warming. Based on our analysis, meltwater is produced for only a fraction of the summer season; we find that melting conditions would occur for up to 30 days. Thus, if we assume that an equal amount of meltwater is produced each day that meltwater is produced in the summer season and that no meltwater is produced outside of the summer season, the daily runoff rate during the summer season would be ~0.6 mm/day, which is likely to be too low to form the observed geomorphology of the valley networks.

Scanlon et al. (2016) studied average daily runoff rates at specific valley networks, finding that more greenhouse warming than considered here is likely to be required to produce intermittent daily runoff rates of mm/day to cm/day. We conclude that, while this seasonal melting mechanism produces the required volumes of water to form the valley networks in the approximate duration of valley network formation, spanning a period of ~10^8 years, runoff rates are likely to be too low to form the observed features, in agreement with Scanlon et al. (2016). Thus, we consider that intermittent episodes of more intense, transient heating, potentially due to impact-induced warming or volcanism-induced warming, may be required to produce the necessary daily runoff rates for the conditions of a circular orbit, regardless of total annual meltwater produced.

3.3.3. Consideration of runoff rates: MAT ~225 K, eccentricity of 0.17, climate scenario

In this analysis, we have considered two perihelion conditions and assumed that, on average, each perihelion condition would have persisted for approximately half of the duration of valley network formation. The two perihelion conditions that we utilized are perihelion at $L_s = 90$, or northern hemispheric summer, and perihelion at $L_s = 270$, or southern hemispheric summer. When conditions are such that perihelion occurs during northern hemispheric summer, conditions suitable to the production of meltwater in the southern latitudes will almost never persist. On the other hand, when conditions are such that perihelion occurs during southern hemispheric summer, conditions suitable to the production of meltwater in the equatorial region and slightly southern latitudes will persist during the summer season and significant volumes of meltwater are produced because most of the predicted Late Noachian ice sheet is in the southern hemisphere.

Thus, when the perihelion scenario permits ($L_s = 270$), significantly higher runoff rates will ensue, and when perihelion precesses to $L_s = 90$, every ~50 ky, little to no meltwater is produced in the regions with abundant valley networks. In other words, higher eccentricity conditions (eccentricity of 0.17; perihelion at $L_s = 90$ and $L_s = 270$) can introduce a ~50 ky intermittency into the production of meltwater in regions with abundant valley networks and, while perihelion occurs at $L_s = 270$, significant meltwater is produced and runoff rates are increased by a factor of approximately two in comparison to runoff rates estimated for circular orbit conditions, producing runoff rates more similar to those estimated by Hoke et al. (2011). The maximum thickness of ice melted in regions with abundant valley networks (when perihelion occurs at $L_s = 270$) is ~30–40 mm/year. Based on our analysis of temperature time series at the three valley network locations, a maximum of ~15 days experiences PDT > 273 K for conditions of perihelion at $L_s = 270$. Thus, if we assume that an equal amount of meltwater is produced in every day that experiences conditions suitable to melting in the summer season, runoff rates would be ~2–2.7 mm/day. This estimate is within the range predicted by Hoke et al. (2011), ~mm/day—cm/day, suggesting that this spin-axis/orbital and atmospheric pressure scenario can reproduce the observed geomorphology of the valley networks.

In conclusion, there are two spin-axis/orbital and pressure conditions that are suitable to the production of the correct volume of meltwater in the correct period of time to be responsible for valley network formation: (1) low obliquity (25°), relatively high atmospheric pressure (1000 mbar CO_2 atmosphere), circular orbit, and additional greenhouse warming (MAT~243 K), and (2) low obliquity (25°), relatively lower atmospheric pressure (600 mbar CO_2 atmosphere), eccentricity of 0.17, and no additional greenhouse warming. However, when considering the former spin-axis/orbital and pressure conditions, the seasonal melting mechanism does not predict high enough runoff rates to form the observed geomorphology of the valley networks when compared to the estimates of required runoff rates for valley network formation from Hoke et al. (2011). On the other hand, if optimal perihelion conditions persisted for summertime melting (e.g. perihelion precesses

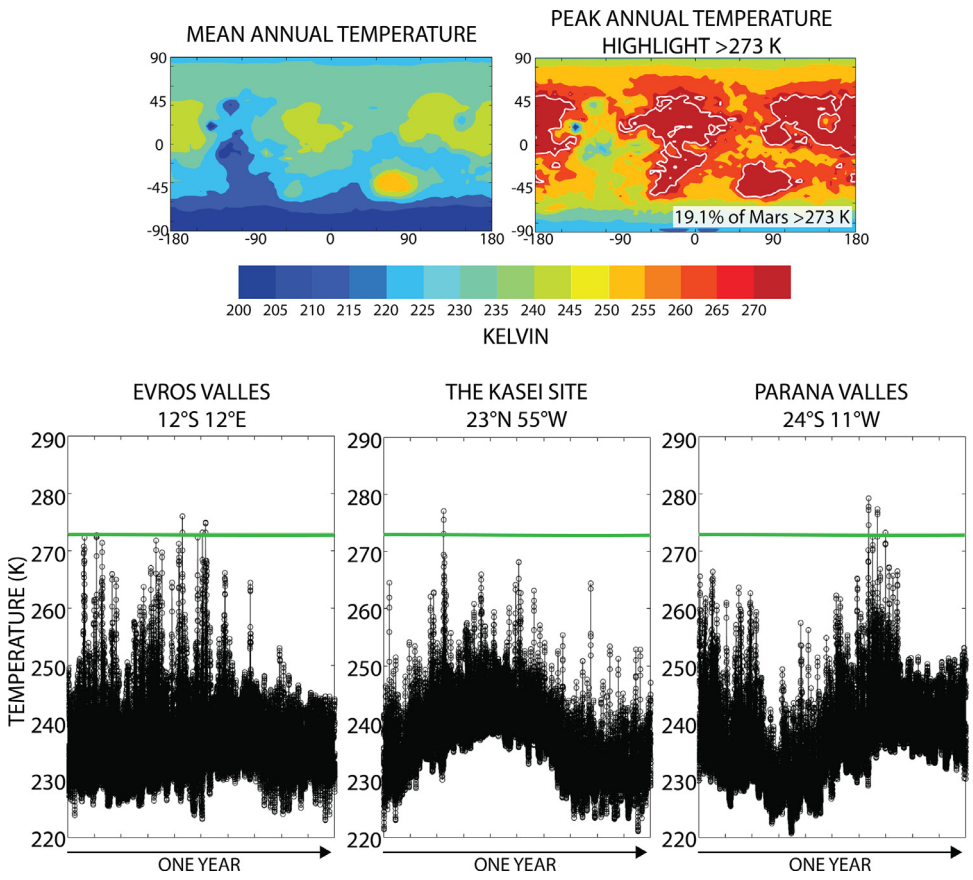

Fig. 12. Results from 15° obliquity analysis. Top: mean annual and peak annual temperature maps. Bottom: temperature time series at three valley network locations. This figure highlights that 15° obliquity will produce less meltwater than 25° obliquity, suggesting that 25° obliquity is the optimal obliquity condition for formation of the valley networks.

between $L_s = 90$ and $L_s = 270$), a ~50 ky intermittency is introduced into the seasonal melting mechanism and, for the duration in which perihelion occurs at $L_s = 270$ and there is significant melting in regions with abundant valley networks, runoff rates are sufficiently high to incise the valley networks. Thus, we conclude that the optimal spin-axis/orbital and atmospheric pressure conditions for valley network formation are low obliquity (25°), relatively low atmospheric pressure (600 mbar), and eccentricity of 0.17. In this scenario, the seasonal melting mechanism is capable of producing meltwater in equatorial regions where valley networks are abundant, producing the necessary volume of water for valley network formation in the corresponding duration of valley network formation (spanning ~10^8 years), and producing runoff rates comparable to those required for valley network incision.

3.4. Additional simulations

In addition to the simulations described above, we have also completed multiple additional simulations to explore fully the possible Noachian climate parameter space. Our previous results suggest that low obliquity, paired with either high atmospheric pressure (1000 mbar) and additional greenhouse warming or lower atmospheric pressure (600 mbar) and relatively high eccentricity (0.17), provide optimal conditions to produce meltwater in the equatorial regions and form the valley networks. Although statistically less likely, it is also possible that obliquity was lower than 25° and eccentricity was higher than 0.17. Thus, we consider a lower obliquity case of 15° and a higher eccentricity case of 0.2, the latter representing the maximum eccentricity that may have existed in the past 5 billion years based on the statistical analysis of Laskar et al. (2004).

3.4.1. 15° obliquity

Here, we consider whether lower obliquity conditions could produce significantly more meltwater in equatorial regions without the necessity of additional greenhouse warming for the case of a circular orbit. We have already shown that high atmospheric pressure is optimal for producing seasonal melting in a "cold and icy" climate under the conditions of a circular orbit, so we explore 15° obliquity, 1000 mbar CO_2 atmosphere, circular orbit, and no additional warming (Fig. 12). In this scenario, PAT > 273 K are focused in the equatorial region; Parana Valles experiences 3 days with PDT > 273 K, Evros Valles experiences 3 days with PDT > 273 K, and the Kasei site experiences 1 day with PDT > 273 K. The major difference between 15° obliquity and 25° obliquity appears to be in the Evros Valles region; the geographic location of Evros Valles is very close to the equator and the lower obliquity focuses more incident solar radiation in that region, increasing the number of days with PDT above freezing. However, the number of days with PDT > 273 K at the other two valley network locations are approximately the same as for the 25° obliquity case, suggesting that a slightly lower obliquity does not cause a significant difference and additional greenhouse warming would be required to produce sufficient meltwater to form the valley networks under these spin-axis/orbital and pressure conditions. The results of a PDD analysis suggest that 1.58×10^8 m^3 (1.89×10^{-6} m GEL) of meltwater is produced annually under these spin-axis/orbital conditions. If 3–100 m GEL of water was required to form the valley networks, it would take

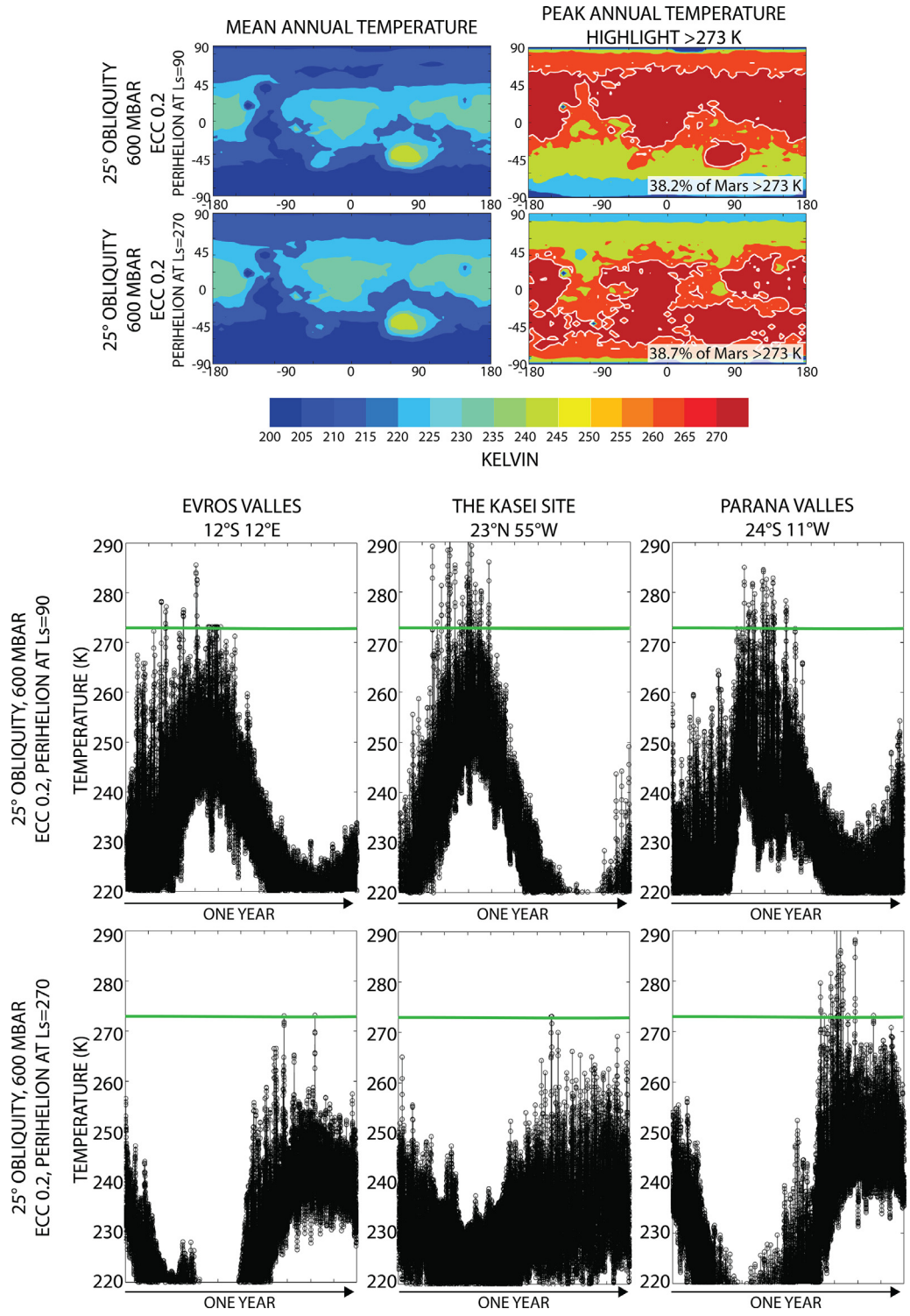

Fig. 13. Results from the analysis of conditions of eccentricity of 0.2. Same as Fig. 12, but for conditions of 25° obliquity and 1000 mbar CO_2 atmosphere. We find that, similar to eccentricity of 0.17, the increased eccentricity leads to the production of significant volumes of meltwater in the equatorial region, suggesting that the valley networks may have formed during a high eccentricity phase in the Noachian. This conclusion suggests that additional warming may not have been required and that the valley networks may have formed in a "cold and icy" (MAT ~225 K) climate.

2,750,000–91,800,000 years to form the valley networks. The upper limit of this range is outside of the estimated timescale for individual valley network formation (10^5–10^7 years; Hoke et al., 2011) and is approximately equal to the upper limit for the duration of formation of all Noachian valley networks (~10^8 years; Hoke et al., 2011). The lower obliquity considered here produces slightly less annual meltwater than the comparable 25°, ambient 1000 mbar CO_2 atmosphere with no additional greenhouse warming, circular orbit scenario (1.83×10^8 m^3), likely because more ice in the southern hemisphere can be melted at the 25° obliquity case, while vast portions of the more equatorial region effected by the 15° obliquity warm conditions are devoid of snow and ice.

Additionally, maximum daily runoff rates under these conditions are less than mm/day, which is likely to be too low to incise the valley networks (Hoke et al., 2011). In summary, although lower obliquity conditions focus the meltwater in the equatorial region where valley networks are abundant, annual volumes of meltwater produced and corresponding runoff rates are likely to be too low to form the valley networks under these spin-axis/orbital conditions.

3.4.2. 0.2 eccentricity

We have shown that relatively high eccentricity (0.17) can increase summertime temperatures significantly to produce meltwater in equatorial regions without additional greenhouse warming. Additionally, under the correct perihelion conditions (perihelion at $L_s = 270$), eccentricity of 0.17 can produce runoff rates that are comparable to those required to form the valley networks. Thus, we consider the maximum possible eccentricity (0.2) that is predicted to have occurred in the past 5 billion years (Laskar et al., 2004) to provide an end-member simulation of the influence of eccentricity on seasonal melting in equatorial regions in the Noachian. Fig. 13 shows MAT and PAT maps and temperature time series for low obliquity (25°), 600 mbar CO_2 atmospheric pressure, eccentricity of 0.2, and perihelion conditions of $L_s = 90$ and $L_s = 270$. The higher eccentricity increases the seasonal cycles even further, producing very warm summertime conditions in the hemisphere that experiences summer at perihelion. The results of our PDD analysis suggest that it would take approximately 20,750–693,500 years to produce sufficient meltwater to form the valley networks. However, similar to the simulations with eccentricity of 0.17, significant meltwater is not produced in regions with abundant valley networks under the conditions when perihelion occurs at $L_s = 90$, suggesting that this estimation is a minimum. In other words, the production of meltwater in equatorial regions where valley networks are abundant only persists for approximately half of the time (when perihelion occurs at $L_s = 270$), suggesting that a duration of up to 1,387,000 years may be required to produce sufficient meltwater to form the valley networks under these spin-axis/orbital and atmospheric pressure conditions. Estimations for runoff rates in these simulations is ~2–3 mm/day, similar to those predicted for conditions of eccentricity of 0.17. Thus, the volume of meltwater produced, the duration to produce sufficient meltwater to form the valley networks, and the predicted runoff rates all agree with the observed geomorphology (Hoke et al., 2011), suggesting that these spin-axis/orbital and atmospheric pressure conditions could have been responsible for valley network formation. However, it is important to note that these results do not differ significantly from those of simulations with eccentricity of 0.17, and an eccentricity of 0.17 was more likely to occur in the past 5 billion years (Laskar et al., 2004). Thus, it is possible to form the valley networks through this seasonal melting mechanism in a "cold and icy" climate without invoking statistically unlikely eccentricity conditions.

4. Discussion and conclusions

In our analysis of the Late Noachian Mars climate model (Wordsworth et al., 2013), we followed the broad exploratory approach of Richardson and Mischna (2005), using improved models (Forget et al., 2013; Wordsworth et al., 2013) to test the "cold and icy highlands" model (Wordsworth et al., 2013, 2015). We addressed the following specific questions and reached the following conclusions:

Nominal cold and icy MAT ~225 K model:

1. In the nominal Late Noachian "cold and icy highlands" climate model (MAT ~225 K), do PAT ever exceed 273 K anywhere on Mars?
   Even with MAT ~225 K, PAT can exceed 273 K in the nominal equilibrium "cold and icy" Noachian Mars climate scenario. Additionally, when considering a circular orbit, low obliquity and high atmospheric pressure conditions (25° obliquity, 1000 mbar CO_2 atmosphere) are optimal for producing PAT > 273 K in the equatorial region where valley networks are abundant (Fig. 2b). Richardson and Mischna (2005) concluded that there would have been a transient liquid water potential (TLWP) "dead zone" between ~0.1 and 1 bar atmospheric pressure. This "dead zone" is defined as conditions during which there are no locations on the planet that have the necessary pressure and temperature conditions for the formation of liquid water. In contrast to this prediction, we find that TLWP conditions, or pressures and temperatures suitable to liquid water, exist in the northern lowlands and other topographic lows, such as the floor of the Hellas impact basin, for all pressure conditions analyzed here, ranging from 600–1000 mbar.
2. In what locations on a "cold and icy" Mars does PAT exceed 273 K?
   We found that PAT exceeds 273 K in broad areas of the northern lowlands and in some equatorial regions, due to the altitude dependence on temperature (Fig. 2b).
3. How do variations in obliquity influence the locations where PAT are >273 K, and their duration?
   It is critical to understand the influence of obliquity on seasonal temperature variation because the obliquity varies through time and it is likely that it was not constant throughout the duration of valley network formation. We explored the obliquity range 25–55° and found that obliquity variations do not influence the percentage of the planet in which PAT > 273 K (when atmospheric pressure is constant), but do cause the distribution of regions with PAT > 273 K to shift poleward at higher obliquities and equatorward at lower obliquities (see Fig. 2b). When considering a circular orbit, there is no trend for changes in duration of temperatures > 273 K at the three valley network locations.
4. How do variations in eccentricity influence the locations and abundance of areas where PAT>273 K?
   We explored the eccentricity range 0–0.17 and found that eccentricity variations do not cause the broad locations of areas where PAT > 273 K to change, but can increase/decrease the size of these areas at relatively extreme eccentricity (Fig. 3b, 5b). We found that at the most extreme eccentricity studied here (0.17; Laskar et al., 2004), areas of Mars where PAT exceeded 273 K ranged from a maximum of ~46% of Mars for a circular orbit, to a maximum of ~71% of Mars for an eccentricity of 0.17. Additionally, increasing the eccentricity allows for the number of days with PAT > 273 K to increase in the hemisphere that experiences summer at perihelion, due to increased summer-season temperatures. Additionally, the longitude of perihelion precession cycle is less than the predicted duration of time required to form simple valley networks (Hoke et al., 2011), suggesting that the longitude of perihelion would change over the course of valley network formation. This suggests that (1) the perihelion scenario where perihelion occurs during southern hemispheric summer, and (2) the perihelion scenario where perihelion occurs during northern hemispheric summer, will each occur during the period of valley network formation. For this reason, we consider the average conditions experienced by the opposing perihelion situations when estimating the ability of this mechanism to produce seasonal meltwater.
5. How do variations in atmospheric pressure influence the location and abundance of areas where PAT >273 K?
   We explored the atmospheric pressure range of 600–1000 mbar and found that atmospheric pressure variations influence the abundance of areas where PAT > 273 K, but do not cause the

distribution to shift. For a circular orbit, we found that for the 25° obliquity case, at 600 mbar, ~22.8% of Mars was characterized by PAT > 273 K, while at 1000 mbar, the percentage of Mars where PAT exceeded 273 K rose to ~28.4% (Fig. 2). However, increasing atmospheric pressure also increases atmospheric thermal blanketing, decreasing the magnitude of the diurnal cycle. We found that this effect is more prominent in more eccentric orbits and the damping of the diurnal cycle has a stronger influence on number of days with PAT > 273 K than the overall MAT increase from the thicker atmosphere. For example, for simulations with 25° obliquity and eccentricity of 0.17, the three valley network locations analyzed here were characterized by more days with PAT > 273 K in simulations with atmospheric pressure of 600 mbar than in simulations with atmospheric pressure of 1000 mbar.

6. For the locations where PAT >273 K, how often does summertime mean seasonal temperature (MST) exceed 273 K?
   We found that despite PAT exceeding 273 K, summertime MST never exceeded 273 K. In other words, the duration of temperatures > 273 K is not long enough to force summer MST to be >273 K when considering a pure CO_2 atmosphere (Fig. 6). Although multiple days in the summer season experience PDT > 273 K, the daily duration of temperatures > 273 K and number of days in the summer season that experience PDT > 273 K is not high enough to increase the summertime MST > 273 K.
7. For the locations where PAT >273 K, how often does peak daytime temperature (PDT) exceed 273 K?
   We found that peak daytime temperatures exceeded 273 K in the northern lowlands and other topographic lows, such as the floor of the Hellas and Argyre basins. During the warmest summertime conditions, PDT at higher altitudes, near the edges of the Noachian ice sheet, may also exceed 273 K. To understand the duration of temperatures > 273 K in regions with abundant valley networks, we performed temperature time-series analyses at three valley network systems (e.g. Fig. 6). The three valley network systems utilized in this study are located at different latitudes and longitudes to represent a global sample. For example, when considering 25° obliquity and 1000 mbar CO_2 atmosphere, we found that PDT exceeded 273 K at the valley networks near the Kasei site for 2 days (~1% of the year) for circular orbital conditions and up to ~9 days (~1.5% of the year) for more eccentric orbital conditions (0.17), when considering the scenario during which perihelion occurs during northern hemispheric summer. This result highlights that the more extreme seasonal cycles characteristic of increased eccentricity can produce more summertime melting in regions with abundant valley networks.
   Specifically, at Lake Hoare in the MDV, ~5–7% of the year above 273 K is necessary to form and sustain the lake, a percentage which is comparable to that observed for the simulations with 25° obliquity, 600 mbar CO_2 atmosphere, and eccentricity of 0.17 (maximum 25 days with PDT > 273 K at the Kasei site (~4% of the year), maximum 30 days with P DT> 273 K at Parana Valles (~4.5% of the year), and maximum 22 days with PDT > 273 K at Evros Valles (~3% of the year); the maximum values are taken as the maximum value from either perihelion scenario). Thus, the percentage of the year during which temperatures exceed freezing at the three valley network systems may be sufficient to produce the necessary volume of meltwater for formation of the valley networks when repeated over many years.
8. For the locations where PDT exceeds 273 K, what percentage of the day does temperature exceed 273 K?
   On average, for the specific valley networks studied here, temperatures above 273 K in the equatorial region do not usually last for more than a few data points per year. At the three valley network systems that we analyzed, for low obliquity (25° obliquity) and high atmospheric pressure (1000 mbar), (1) for the case of a circular orbit, on average 0–2 days have PDT > 273 K and only one to two hours are characterized by temperature > 273 K on each of those days, and (2) for the case of a more eccentric orbit (0.17), 0–30 days have PDT > 273 K and on average three to four hours are characterized by temperature > 273 K on each of those days.
9. Are the locations where PAT exceeds 273 K also locations where snow and ice is predicted to occur in the "cold and icy" climate model?
   We compared the locations where PAT exceeds 273 K with the locations of snow and ice predicted by the "Late Noachian Icy Highlands" model (Fig. 4; circular orbit) and found a close correspondence in the equatorial and near equatorial regions, especially for lower obliquity conditions (25°). For example, some regions of PAT > 273 K appear to correspond well with the edges of the predicted ice sheet, producing a small amount of annual melting in these areas (Fig. 11). The fluvial and lacustrine features correlate well with this distribution; they are located at the edges of the ice sheet where melting and runoff would be expected to occur if durations were sufficient. For a circular orbit and pure CO_2 atmosphere, we interpret durations of conditions suitable to melting of surface ice to be insufficient at all valley network locations analyzed in this study. For a more eccentric orbit (eccentricity of 0.17), durations of melting conditions at the three valley network systems are comparable to durations observed in the Antarctic Dry Valleys: valley networks north of the equator would have formed when perihelion occurred during northern hemispheric summer and valley networks south of the equator would have formed when perihelion occurred during southern hemispheric summer. For both a circular orbit and more eccentric orbit, areas in the northern lowlands where PAT is predicted to exceed 273 K are devoid of snow and ice, and the duration of temperatures > 273 K appears to be insufficient to penetrate the dry permafrost and to cause significant melting of ice-cemented permafrost.
10. Are the periods of time during which PDT exceeds 273 K of sufficient length to cause top-down melting of snow and ice and runoff?
    We found that the average number of days with PDT > 273 K globally are of sufficient duration to cause top-down melting of snow and ice and runoff of water to create fluvial and lacustrine activity. When considering a circular orbit, our simulations suggest that an area of up to ~45% of Mars could be exposed to temperatures > 273 K during peak daytime conditions for many days during the summer season. It is important to note, however, that a large portion of this ~45% is located in the northern lowlands, a region predicted to be devoid of snow and ice. When focusing on specific valley networks, we find that the possibility of warm temperatures (and their duration) in these (more equatorial) regions is low. For pure CO_2 atmospheric conditions and a circular orbit, the duration of temperatures > 273 K at these locations may be insufficient to permit liquid water fluvial and lacustrine processes to operate long enough before refreezing of the stream and lake surfaces. Additionally, melt volume calculations suggest that this process would have to repeat for hundreds of millions of years to form the valley networks. Hoke et al. (2011) estimate that individual valley networks were likely to have formed in ~10^5–10^7 years and all valley networks formed between 3.6 and 3.8 Gya, suggesting that this process may be insufficient because the amount of time required to produce enough meltwater to carve the valley networks extends to the upper limit of this predicted time range. Lastly, runoff rates produced by this seasonal

melting mechanism would be significantly lower than those estimated to be necessary to form the observed valley networks (Hoke et al., 2011).

However, we also analyzed the influence of increased eccentricity and find that increased eccentricity can significantly affect the seasonal cycle in the equatorial region and that, because Mars would experience both perihelion situations within $\sim 10^8$ years, valley networks in both the southern and northern hemisphere would experience warm conditions comparable to what is observed in the Antarctic Dry Valleys at least half of the time. Because the predicted ice sheet is distributed mostly within the southern hemisphere, most ice melting occurs under the conditions when perihelion occurs during southern hemispheric summer occurs. For eccentricity of 0.17, this seasonal melting process would be required to persist for a minimum of 32,500–1,083,000 years to form the valley networks, within the range predicted by Hoke et al. (2011). Additionally, runoff rates produced through this seasonal melting mechanism are similar to those required for valley network formation (~mm/day). This is due to the enhanced southern hemispheric summertime melting when orbital conditions are such that perihelion occurs at $L_s = 270$. For these reasons, we believe that the valley networks could have been formed through this seasonal melting mechanism when Mars experienced high eccentricity conditions.

Nominal cold and icy MAT ~225 K model with gray-gas induced ~18 K temperature increase:

1. Are greenhouse gases required to induce higher temperatures in order to explain the observed valley networks and closed/open-basin lakes in a "cold and icy" early Mars climate? For the conditions of a circular orbit, we have shown that the locations and duration of PDT > 273 K in a "cold and icy" early Mars climate are sufficient to induce limited top-down heating and melting in some regions, but it may not be of sufficient annual duration to form all of the observed fluvial and lacustrine surface features. However, with the addition of modest greenhouse warming, durations of temperatures > 273 K are significantly increased, and PDT > 273 K are produced for at least ~1% of the year (~8 days) at all studied valley networks locations (Fig. 10).

Melt volume calculations suggest that the optimal spin-axis conditions for producing snowmelt and runoff in the equatorial region when considering a circular orbit are 25° obliquity, 1000 mbar CO_2 atmosphere, and additional greenhouse warming (globally averaged MAT ~18 K increase; $\kappa = 2.5 \times 10^{-5}$ m^2 kg^{-1}). Under these conditions, the melt distribution correlates well with the valley network distribution and the seasonal melting process would need to repeat for ~20,700–548,000 years to form the valley networks.

Additionally, Wordsworth et al. (2017) have explored the potential of warming a reduced atmosphere on Mars and find that collision induced absorption (CIA) warming effects (namely CO_2–CH_4 and CO_2–H_2) have been underestimated in the past. Producing the necessary ~18 K globally averaged MAT increase might be accomplished through CIA effects, for example, requiring the addition of a smaller amount of greenhouse gases in the atmosphere than when underestimating CIA effects, as has been done in the past.

While this mechanism can produce the necessary volume of water to erode the valley networks within $\sim 10^5$ years, it is possible that runoff rates may be too low to match the observed geomorphology of the valley networks (Hoke et al., 2011), implying that warmer temperatures or other external heating mechanisms may be required if the eccentricity in the Noachian was circular (or significantly lower than 0.17).

Main conclusion:

There are four necessary requirements to form the valley networks through transient heating and ice melting in a cold and icy climate. (1) Melting of ice must occur in the equatorial region where valley networks are abundant. This requires the presence of both ice and temperatures above 273 K. (2) The melting process must persist, either continuously or in transient periods, for the estimated duration of valley network formation ($\sim 10^5$–10^7 years for individual valley networks, $\sim 10^8$ years to form all Noachian valley networks; Hoke et al., 2011). (3) Within this time period, the predicted volume of meltwater produced must be comparable to the necessary amount for valley network formation (3–100 m GEL; Rosenberg and Head, 2015). (4) Runoff rates of the meltwater must be comparable to the required runoff rates inferred from geomorphological observations of the valley networks (Hoke et al., 2011).

We conclude that it is possible to meet the first three of these requirements for formation of the valley networks through seasonal melting for conditions of (1) low obliquity (25°), high atmospheric pressure (1000 mbar), a circular orbit, and a small amount of additional greenhouse warming (MAT ~243 K), or (2) low obliquity (25°), relatively lower atmospheric pressure (600 mbar), eccentricity of 0.17, and no additional greenhouse warming. We favor the latter conditions because these conditions also produce the necessary runoff rates to incise the valley networks (the fourth requirement). The former conditions produce runoff rates that are likely too low to form the observed geomorphology of the valley networks; future analyses are required to determine whether lower runoff rates than those previously estimated by Hoke et al. (2011) could be sufficient to form the valley networks.

In conclusion, neither "warm and wet" ambient conditions (MAT ~273 K) nor external forcing, such as impact cratering or volcanism to drive the MAT to 273 K, are required to form the valley networks; seasonal melting could potentially form the valley networks in a "cold and icy" climate, specifically under the conditions of a more eccentric orbit.

Conclusions from additional simulations:

1. Does lower obliquity produce more equatorial melting?
   Our initial analysis suggests that low obliquity (25°) is critical for the production of meltwater in the equatorial regions where valley networks are abundant. We considered 15° obliquity to determine whether lower obliquities than those considered in our original analysis would focus temperatures > 273 K even closer to the equator, possibly aiding in valley network formation. Our original simulations did not include this obliquity condition because it is outside of the $\pm 1\sigma$ range from the estimated average obliquity for the past 5 billion years (~25–55° obliquity; Laskar et al., 2004). However, it is important to consider lower obliquity conditions as well because, although less likely, these lower obliquity conditions may have persisted for a significant period of time during martian history, as well. We find that 15° obliquity produces less meltwater than the 25° obliquity simulation. This is likely to be because 15° obliquity implies that maximum solar insolation is very close to the equator, but the predicted "Late Noachian Icy Highlands" ice sheet and valley networks do not perfectly align with the equator. In fact, a significant portion of the ±15° latitudinal band is ice-free. Thus, we have confirmed that 25° obliquity is the optimal obliquity condition for equatorial melting and valley network formation.
2. Does increasing eccentricity further produce even more annual meltwater?
   We find that the simulations with eccentricity of 0.2 produce significant meltwater, similar to the simulations with eccentricity of 0.17. The higher eccentricity produces a stronger seasonal cycle, suggesting that (1) when the perihelion condition is

such that perihelion occurs during southern hemispheric summer, there is significant ice melting and the valley networks in the southern hemisphere experience a percentage of the year with PDT > 273 K comparable to what is observed in the Antarctic Dry Valleys, and (2) a similar scenario occurs in the northern hemisphere when the perihelion condition is such that the northern hemisphere experiences summer closer to perihelion, but much less meltwater is produced because a significant portion of the northern hemisphere is devoid of snow and ice. Under these conditions, the necessary volume of meltwater to incise the valley networks is produced within the estimated time duration for formation of individual valleys (Hoke et al., 2011) and estimated runoff rates are similar to predicted rates for valley network incision (Hoke et al., 2011). However, the results presented for eccentricity of 0.2 are not much different than those for eccentricity of 0.17; the higher, less likely, eccentricity value (0.2) is not required to form the valley networks. We conclude that a period of increased eccentricity on Mars may have been responsible for elevating seasonal temperatures in the equatorial region, producing significant meltwater, and incising the valley networks in an ambient "cold and icy" climate.

In summary, these results underline the critical importance of PAT, PDT and PST, in addition to MAT. Our results underline the fact that MAT does not need to exceed 273 K in order to explain the activity associated with the observed fluvial and lacustrine features. We conclude that there are two spin-axis/orbital and atmospheric pressure scenarios that could be responsible for Noachian valley network formation: (1) low obliquity (25°), relatively high atmospheric pressure (1000 mbar), circular orbit, and a modest amount of additional greenhouse warming, or (2) low obliquity (25°), relatively lower atmospheric pressure (600 mbar), no additional greenhouse warming, and higher eccentricity conditions (0.17). However, the former scenario cannot reproduce the necessary runoff rates to form the observed geomorphology of the valley networks, so we conclude that the latter spin-axis/orbital and atmospheric pressure scenario is a better candidate for valley network formation. If climate models have great difficulty in achieving conditions in which MAT exceeds 273 K, then an alternative scenario to that of continuous "warm and wet" conditions could be a combination of (1) modest warming by greenhouse gases, other transient warming mechanisms, or a period of increased eccentricity, and (2) annually repeated summertime seasonal melting of snow and ice to explain the observed fluvial and lacustrine features.

Acknowledgments

The authors would like to thank Dr. Michael Mischna and an anonymous reviewer for their helpful comments and suggestions that have significantly improved this manuscript.

References

Atkins, C.B., Dickinson, W.W., 2007. Landscape modification by meltwater channels at margins of cold-based glaciers, Dry Valleys, Antarctica. Boreas 36, 47–55.
Boucher, O., Treut, H., Baker, M., 1995. Precipitation and radiation modeling in a general circulation model: introduction of cloud microphysical processes. J. Geophys. Res. 100(D8) (16), 395–414.
Carr, M., 1999. Retention of an atmosphere on early Mars. J. Geophys. Res.: Planets 104 (E9), 21897–21909.
Cassanelli, J., Head, J., Fastook, J., 2015. Sources of water for the outflow channels on Mars: implications of the Late Noachian "icy highlands" model for melting and groundwater recharge on the Tharsis rise. Planet. Space Sci. 108, 54–65.
Chinn, T.J.H., 1986. Structure and equilibrium of the Dry Valley glaciers. New Zealand Antarctic Rec. 6, 73–88.
Clifford, S., Parker, T., 2001. The evolution of the martian hydrosphere: implications for the fate of a primordial ocean and the current state of the northern plains. Icarus 154, 40–79.
Clow, G., 1987. Generation of liquid water on Mars through the melting of a dusty snowpack. Icarus 72, 95–127.
Craddock, R., Howard, A., 2002. The case for rainfall on a warm, wet early mars. J. Geophys. Res. 107, 5111.
Fassett, C., Head, J., 2008a. The timing of martian valley network activity: constraints from buffered crater counting. Icarus 195, 61–89.
Fassett, C., Head, J., 2008b. Valley network-fed, open-basin lakes on Mars: distribution and implications for Noachian surface and subsurface hydrology. Icarus 198, 37–56.
Fastook, J., Head, J., 2015. Glaciation in the Late Noachian Icy Highlands: ice accumulation, distribution, flow rates, basal melting, and top-down melting rates and patterns. Planet. Space Sci. 106, 82–98.
Fenton, L., Richardson, M., 2001. Martian surface winds: insensitivity to orbital changes and implications for aeolian processes. J. Geophys. Res. 106, 885–902.
Forget, F., Wordsworth, R., Millour, E., Madeleine, J-B., Kerber, L., Leconte, J., Marcq, E., Haberle, R., 2013. 3D modelling of the early martian climate under a denser CO_2 atmosphere: temperatures and CO_2 ice clouds. Icarus 222, 81–99.
Fountain, A.G., Lewis, K.J., Doran, P.T., 1999. Spatial climatic variation and its control on glacier equilibrium line altitude in Taylor Valley, Antarctica. Global Planet. Change 22, 1–10.
Gooseff, M., Barrett, J., Adams, B., Doran, P., Fountain, A., Lyons, W.B., McKnight, D., Priscu, J, Sokol, E., Takacs-Vesbach, C., Vandegehuchte, M., Virginia, R., Wall, D., 2017. Decadal ecosystem response to an anomalous melt season in a polar desert in Antarctica. Nat. Ecol. Evol. doi:10.1038/s41559-017-0253-0.
Goudge, T., Mustard, J., Head, J., Salvatore, M., Wiseman, S., 2015. Integrating CRISM and TES hyperspectral data to characterize a halloysite-bearing deposit in Kashira crater, Mars. Icarus 250, 165–187.
Gough, D., 1981. Solar interior structure and luminosity variations. Sol. Phys 74, 21–24.
Halevy, I., Head, J., 2014. Episodic warming of early Mars by punctuated volcanism. Nat. Geosci. Lett. doi:10.1038/NGEO2293.
Halevy, I., Zuber, M., Schrag, D., 2007. A sulfur dioxide climate feedback on early Mars. Science 318, 1903–1907.
Head, J., Marchant, D., 2014. The climate history of early Mars: insights from the Antarctic McMurdo Dry Valleys hydrologic system. Antarctic Sci. 26 (6), 774–800.
Hoke, M., Hynek, B., Tucker, G., 2011. Formation timescales of large Martian valley networks. Earth Planet. Sci. Lett. 312, 1–12.
Hourdin, F., 1992. A new representation of the absorption by the CO_2 15-micron band for a Martian general circulation model. J. Geophys. Res. 97 (18), 319–335.
Huybrechts, P., Letreguilly, A., Reeh, N., 1991. The Greenland ice sheet and greenhouse warming. Global Planet. Change 3, 399–412.
Hynek, B., Beach, M., Hoke, M., 2010. Updated global map of Martian valley networks and implications for climate and hydrologic processes. J. Geophys. Res.: Planets 115, E09008.
Johnson, S., Mischna, M., Grove, T., Zuber, M., 2008. Sulfur-induced greenhouse warming on early Mars. J. Geophys. Res. Planets 113, 8005.
Kasting, J.K., 1991. CO_2 condensation and the climate of early Mars. Icarus 94, 1–13.
Kasting, J., Brown, L., Accord, J., Pollack, J., 1992. Was early Mars warmed by ammonia? In: Haberle, R.M., Jakosky, B.M. (Eds.) Martian Surface and Atmosphere through Time, pp. 84–85.
Kerber, L., Forget, F., Wordsworth, R., 2015. Sulfur in the early martian atmosphere revisited: experiments with a 3-d global climate model. Icarus 261, 133–148.
Kite, E., Halevy, I., Kahre, M., Wolff, M., Manga, M., 2013. Seasonal melting and the formation of sedimentary rocks on Mars, with predictions for the Gale Crater mount. Icarus 223, 181–210.
Kuhn, W., Atreya, S., 1979. Ammonia photolysis and the greenhouse effect in the primordial atmosphere of the Earth. Icarus 37, 207–213.
Kreslavsky, M., Head, J., 2000. Kilometer-scale roughness of Mars: results from MOLA data analysis. J. Geophys. Res. 105 (E11). 26, 695–26, 711.
Kreslavsky, M., Head, J., 2003. North-south topographic slope asymmetry on Mars: evidence for insolation-related erosion at high obliquity. Geophys. Res. Lett. 30 (15), 1815. doi:10.1029/2003GL017795.
Kreslavsky, M., Head, J., 2006. Modification of impact craters in the northern plains of Mars: implications for the Amazonian climate history. Meteorit. Planet. Sci. 41, 1633–1646.
Laskar, J., Correia, A, Gastineau, M., Joutel, F., Levrard, B., Robutel, P., 2004. Long term evolution and chaotic diffusion of the insolation quantities of Mars. Icarus 170, 343–364.
Marchant, D., Head, J., 2007. Antarctic dry valleys: microclimate zonation, variable geomorphic processes, and implications for assessing climate change on Mars. Icarus 192, 187–222.
Mischna, M.M., Richardson, R.Wilson, McCleese, D., 2003. On the orbital forcing of Martian water and CO_2 cycles: a general circulation model study with simplified volatile schemes. J. Geophys. Res. 108 (E6), 5062.
Mischna, M., Baker, V., Milliken, R., Richardson, M., Lee, C., 2013. Effects of obliquity and water vapor/trace gas greenhouses in the early martian climate. J. Geophys. Res.: Planets 118, 560–576.
Palumbo, A., Head, J., 2017a. Impact cratering as a cause of climate change and the effects on dating of surfaces on Late Noachian Mars. Meteorit. Planet. Sci. in press.
Palumbo, A., Head, J., 2017b. An analysis of seasonal temperature variation in the Antarctic McMurdo Dry Valleys: Implications for early martian climate and valley network formation. *Lunar and Planetary Science Conference* 48 Abstract 2192.
Postawko, S., Kuhn, W., 1986. Effect of the greenhouse gases (CO_2, H_2O, SO_2) on Martian paleoclimate. J. Geophys. Res. 91, D431–D438.
Richardson, M., Mischna, M., 2005. Long-term evolution of transient liquid water on Mars. J. Geophys. Res. 110, E03003.

Richardson, M., Wilson, R., 2002. Investigation of the nature and stability of the Martian seasonal water cycle with a general circulation model. J. Geophys. Res. 107 (E5), 5031.
Rosenberg, E., Head, J., 2015. Late Noachian fluvial erosion on Mars: cumulative water volumes required to carve the valley networks and grain size of bed-sediment. Planet. Space Sci. 117, 429–435.
Sagan, C., Chyba, C., 1997. The early faint young sun paradox: organic shielding of ultraviolet-labile greenhouse gases. Science 276, 1217–1221.
Sagan, C., Mullen, G., 1972. Earth and Mars: evolution of atmospheres and surface temperatures. Science 177, 52–56.
Scanlon, K., Head, J., Wordsworth, R., 2016. Modeled snowmelt rates in early Martian climate scenarios. Icarus in press.
Segura, T., Toon, O., Colaprete, A., Zahnle, K., 2002. Environmental effects of large impacts on Mars. Science 298, 1977–1980.
Segura, T., Toon, O., Colaprete, A., 2008. Modeling the environmental effects of moderate-sized impacts on Mars. J. Geophys. Res. 113, E11007.
Segura, T., McKay, C., Toon, O., 2012. An impact-induced, stable, runaway climate on Mars. Icarus 220, 144–148.
Toon, O., Segura, T., Zahnle, K., 2010. The formation of martian river valleys by impacts. Earth Planet. Sci. 38, 303–322.
Wilson, L., Head, J., 2009. Tephra deposition on glaciers and ice sheets on Mars: Influence on ice survival, debris content and flow behavior. J. Volcanol. Geotherm. Res. 185, 290–297.
Wolf, E., Toon, O., 2010. Fractal organic hazes provided an ultraviolet shield for early Earth. Science 328, 1266.
Wilson, R.J., Hamilton, K.P., 1996. Comprehensive model simulation of thermal tides in the Martian atmosphere. J. Atmos. Sci. 53, 1290–1326.
Wilson, R.J., Richardson, M.I., 2000. The Martian atmosphere during the Viking mission, I. Infrared measurements of atmospheric temperatures revisited. Icarus 145, 555–579.
Wordsworth, R., Kalugina, Y., Lokshtanov, S., Vigasin, A., Ehlmann, B., Head, J., Sanders, C., Wang, H., 2017. Transient reducing greenhouse warming on early Mars. Geophys. Res. Lett. 44 (2), 665–671.
Wordsworth, R., 2016. The climate of early Mars. Annu. Rev. Earth Planet. Sci. 44, 1–31.
Wordsworth, R., Forget, F., Millour, E., Head, J., Madeleine, J.-B., Charnay, B., 2013. Global climate modelling of early martian climate under a denser CO_2 atmosphere: water cycle and ice evolution. Icarus 222 (1), 1–19.
Wordsworth, R., Kerber, L., Pierrehumbert, R., Forget, F., Head, J., 2015. Comparison of “warm and wet” and “cold and icy” scenarios for early Mars in a 3-D climate model. J. Geophys. Res.: Planets 120, 1201–1219.